Somatic Mutations in *TSC1* and *TSC2* Cause Focal Cortical Dysplasia

Jae Seok Lim,[1,13] Ramu Gopalappa,[2,3,13] Se Hoon Kim,[4,13] Suresh Ramakrishna,[2] Minji Lee,[5] Woo-il Kim,[1] Junho Kim,[7] Sang Min Park,[1] Junehawk Lee,[8] Jung-Hwa Oh,[9] Heung Dong Kim,[10] Chang-Hwan Park,[2] Joon Soo Lee,[10] Sangwoo Kim,[7] Dong Seok Kim,[11] Jung Min Han,[5,6] Hoon-Chul Kang,[10,14] Hyongbum (Henry) Kim,[3,7,12,14,*] and Jeong Ho Lee[1,14,*]

Focal cortical dysplasia (FCD) is a major cause of the sporadic form of intractable focal epilepsies that require surgical treatment. It has recently been reported that brain somatic mutations in *MTOR* account for 15%–25% of FCD type II (FCDII), characterized by cortical dyslamination and dysmorphic neurons. However, the genetic etiologies of FCDII-affected individuals who lack the *MTOR* mutation remain unclear. Here, we performed deep hybrid capture and amplicon sequencing (read depth of 100×–20,012×) of five important mTOR pathway genes—*PIK3CA, PIK3R2, AKT3, TSC1,* and *TSC2*—by using paired brain and saliva samples from 40 FCDII individuals negative for *MTOR* mutations. We found that 5 of 40 individuals (12.5%) had brain somatic mutations in *TSC1* (c.64C>T [p.Arg22Trp] and c.610C>T [p.Arg204Cys]) and *TSC2* (c.4639G>A [p.Val1547Ile]), and these results were reproducible on two different sequencing platforms. All identified mutations induced hyperactivation of the mTOR pathway by disrupting the formation or function of the TSC1-TSC2 complex. Furthermore, in utero CRISPR-Cas9-mediated genome editing of *Tsc1* or *Tsc2* induced the development of spontaneous behavioral seizures, as well as cytomegalic neurons and cortical dyslamination. These results show that brain somatic mutations in *TSC1* and *TSC2* cause FCD and that in utero application of the CRISPR-Cas9 system is useful for generating neurodevelopmental disease models of somatic mutations in the brain.

Introduction

Focal cortical dysplasia (FCD) is the most common cause of drug-resistant epilepsy in children who require epilepsy surgery as a treatment.[1,2] FCD is diagnosed in 20%–25% of individuals who undergo epilepsy surgery.[3–5] In addition, up to 40% of individuals with FCD continue to experience seizures even after surgical resection of the epileptic focus.[6] Among FCD subtypes, FCD type II (FCDII), which is characterized by cortical dyslamination and dysmorphic neurons such as cytomegalic neurons (FCDIIa) and balloon cells (FCDIIb), is a major form of FCD and accounts for 30%–50% of FCD with surgical treatment[1,3] (Figure 1A). Because the molecular genetic etiology of FCD has remained elusive, genetically validated drug targets in individuals with FCD are poorly understood. Recently, we and another group have shown that somatic activating mutations in *MTOR* (MIM: 601231) in the brain account for 15%–25% of individuals with FCDII[8,9] and that inhibition of hyperactivated mTOR kinase reverses epilepsy and the development of cytomegalic neurons.[8] However, the genetic causes underlying the development of FCDII in individuals who are negative for *MTOR* mutations remain elusive.

The mTOR pathway plays a critical role in the growth of axons and dendrites, synaptic plasticity, and neuronal migration.[10,11] Importantly, mTOR integrates input from a number of upstream signaling pathways involved in the control of cellular growth and metabolism, such as the phosphatidylinositol-3-kinase (PI3K)/AKT and tuberous sclerosis complex (TSC) pathways[12] (Figure S1). Considering that the mTOR kinase is an integrating center for various signals, variants of the upstream regulators of mTOR are likely to affect its activity. In addition, TSC (MIM: 191100) and hemimegalencephaly (HME) are known to share several pathological characteristics with FCDII, such as cytomegalic neurons and epilepsy, and to be linked to aberrantly hyperactivated mTOR signaling.[13–16] Interestingly, TSC and HME are caused by germline or somatic mutations in upstream regulators of mTOR kinase, including *PIK3CA* (MIM: 171834), *PIK3R2* (MIM: 603157), *AKT3* (MIM: 611223), *TSC1*

[1]Brain Korea 21 Plus Project, Graduate School of Medical Science and Engineering, Korea Advanced Institute of Science & Technology, Daejeon 34141, South Korea; [2]Graduate School of Biomedical Science and Engineering, Hanyang University, Seoul 04763, South Korea; [3]Brain Korea 21 Plus Project for Medical Sciences, Graduate Program of Nano Science and Technology, Department of Pharmacology, Yonsei University College of Medicine, Seoul 03722, South Korea; [4]Department of Pathology, Yonsei University College of Medicine, Seoul 03722, South Korea; [5]Department of Integrated OMICS for Biomedical Science, Yonsei University, Seoul 03722, South Korea; [6]College of Pharmacy, Yonsei University, Seoul 03722, South Korea; [7]Severance Biomedical Science Institute, Yonsei University College of Medicine, Seoul 03722, South Korea; [8]Biomedical HPC Technology Research Center, Korea Institute of Science and Technology Information, Daejeon 34141, South Korea; [9]Department of Predictive Toxicology, Korea Institute of Toxicology, Daejeon 34114, South Korea; [10]Division of Pediatric Neurology, Department of Pediatrics, Pediatric Epilepsy Clinics, Severance Children's Hospital, Epilepsy Research Institute, Yonsei University College of Medicine, Seoul 03722, South Korea; [11]Pediatric Neurosurgery, Severance Children's Hospital, Department of Neurosurgery, Yonsei University College of Medicine, Seoul 03722, South Korea; [12]Center for Nanomedicine, Institute for Basic Science, Yonsei University, Seoul 03722, South Korea
[13]These authors contributed equally to this work
[14]These authors contributed equally to this work
*Correspondence: hkim1@yuhs.ac (H.K.), jhlee4246@kaist.ac.kr (J.H.L.)
http://dx.doi.org/10.1016/j.ajhg.2017.01.030.

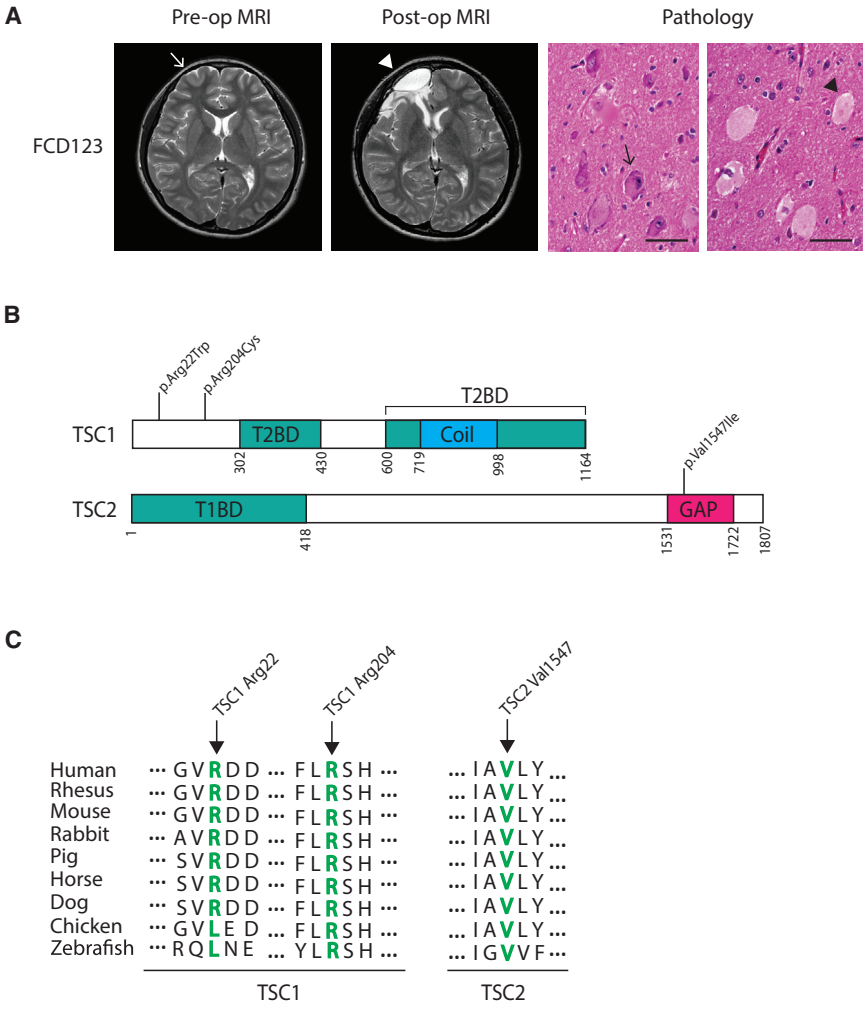

Figure 1. Identification of Brain Somatic Mutations in *TSC1* and *TSC2* in FCDII Individuals Lacking *MTOR* Mutations

(A) Pre- and post-operative brain MRI and H&E staining of pathological samples from FCDII individuals negative for *MTOR* mutations. The white arrow and arrowhead indicate the cortical dysplasia and resected brain regions, respectively. The black arrow and arrowhead indicate dysmorphic neurons and balloon cells (FCDIIb), respectively. Scale bars, 100 μm.

(B) Domain organization and identified mutations in TSC1 and TSC2. A recent study showed that the C terminus of TSC1 binds to the N terminus of TSC2.[7] Abbreviations are as follows: T2BD, TSC2-binding domain; T1BD, TSC1-binding domain; coil, predicted coiled-coil domain; and GAP, GTPase-activating protein domain.

(C) The identified mutation sites in *TSC1* and *TSC2* encode evolutionarily conserved residues.

(MIM: 605284), and *TSC2* (MIM: 191092).[17–19] Moreover, recent studies have reported that mosaic *TSC1* or *TSC2* mutations identified in blood and saliva can cause the milder clinical features of TSC.[20,21] Therefore, it is likely that somatic mutations in genes encoding these upstream regulators of mTOR kinase could be responsible for the development of FCDII in individuals who lack *MTOR* mutations.

In vivo modeling of brain somatic mutations has been a daunting project, mainly because of the lack of proper tools to create somatic mutations in the focal area of the developing animal brain. One method is to use a site-specific recombinase such as Cre recombinase. Plasmid-mediated introduction of Cre recombinase in floxed mice with loxP leads to the generation of a somatic mutation in the brain.[22] However, this Cre-loxP-mediated mutation requires the generation of loxP floxed mice and/or complex crossing of genetically modified mice, which is time consuming and laborious. The development of an easier and more convenient method for the generation of the somatic mutations found in the brain of individuals with neurodevelopmental disorders would greatly facilitate research investigating the molecular pathogenesis and the development of therapeutic modalities for these diseases. The CRISPR (clustered regularly interspaced short palindromic repeats)-Cas9 (CRISPR-associated protein 9) system is becoming widely used to efficiently and accurately edit the genome in vitro and in vivo.[23] We and other groups have also used the CRISPR-Cas9 system to edit the genome in cultured mammalian cells and embryos.[24] By adopting the CRISPR-Cas9 system in the developing mouse brain, it seems possible to model brain somatic mutations and related neurobehavioral deficits in genetically unmodified wild-type mice. Thus, we sought to identify brain somatic mutations in five upstream regulators of mTOR kinase (*PIK3CA*, *PIK3R2*, *AKT3*, *TSC1*, and *TSC2*) in *MTOR*-mutation-negative individuals with FCDII by using deep targeted sequencing strategies and to examine their pathological consequences at the in vivo level by modeling CRISPR-Cas9-mediated somatic mutations in focal cortical regions of the developing mouse brain.

Material and Methods

Subject Ascertainment

FCDII-affected individuals who had undergone epilepsy surgery since 2004 were identified through Severance Children's Hospital. Enrolled individuals met the study entry criteria for FCDII[25] and underwent extensive presurgical evaluations—including video-electroencephalography (video-EEG) monitoring, high-resolution MRI, fluorodeoxyglucose positron emission tomography (FDG-PET), and subtraction ictal single-photon emission computed tomography (SPECT) co-registered to MRI (SISCOM)—to localize anatomic lesions. The presurgical and surgical protocols have been published previously.[26] The resection margin for epilepsy

of the neocortical origin was defined by (1) the presence of a massive and exclusive ictal-onset zone confirmed by intracranial EEG; (2) various interictal intracranial EEG findings, including more than three repetitive spikes per second, runs of repetitive spike and slow wave discharges, localized or spindle-shaped fast activities, and electrodecremental fast activities; and (3) the absence of the eloquent cortex. Complete resection was defined by resection of all areas with seizure-onset and irritative zones on intracranial EEG. The pathological diagnosis of studied individuals with FCDII was reconfirmed for this study according to the recent consensus classification by the International League Against Epilepsy Diagnostic Methods Commission.[25] For all individuals in whom brain somatic mutations in *TSC1* or *TSC2* were identified, we thoroughly evaluated representative organ systems commonly affected by TSC according to surveillance recommendations for suspected TSC.[27] The study was performed and all human tissues were obtained in accordance with protocols approved by Severance Children's Hospital and the Korea Advanced Institute of Science and Technology (KAIST) Institutional Review Board and Committee on Human Research. Informed consent was obtained from the parents of individuals with FCD.

DNA Extraction from Tissue Samples

Genomic DNA was extracted from saliva or formalin-fixed paraffin-embedded (FFPE) brain tissues. The QIAmp DNA FFPE Tissue Kit (QIAGEN) was used for FFPE brain tissues according to the manufacture's protocol. Saliva DNA was extracted with the prepIT•L2P purification kit (DNA Genotek) according to the purification protocol. In brief, 750 μL of mixture from the DNA collection kit (DNA Genotek) was incubated overnight at 50°C in a water incubator. 30 μL of prepIT•L2P solution was added to the mixture. The mixture was centrifuged, and the supernatant was transferred to a fresh tube. 900 μL of 100% ethanol was added to the clear supernatant. The precipitated DNA was centrifuged and collected as a pellet. The ethanol supernatant was discarded, and the DNA pellet was rehydrated in Tris-EDTA (TE) buffer.

Targeted Hybrid Capture and PCR-Based Amplicon Sequencing

We designed hybrid capture probes and amplicon primers including *PIK3CA*, *PIK3R2*, *AKT3*, *TSC1*, and *TSC2* by using SureDesign online tools (Agilent Technologies) and Illumina DesignStudio (Illumina), respectively. We performed library preparation according to the manufacturers' protocol. The final libraries of hybrid capture and PCR-based amplicon sequencing were sequenced on an Illumina HiSeq 2500 (median read depth of 483×) and an Illumina MiSeq (median read depth of 1,348×), respectively.

Bioinformatic Analysis

To generate analysis-ready BAM files from FASTQ files, we used the "Best Practices" workflow suggested by the Broad Institute. We aligned raw sequence from the FASTQ files to the hg19/GRCh37 assembly of the human genome reference sequence by using the Burrows-Wheeler Aligner (BWA-MEM). Detailed bioinformatic analysis for detecting identified mutations is described in Figure S2. For analysis of mutant allele frequencies in the exome database, we adopted standard practices and controls used by a similar study.[28] A total of 2,508 aligned CRAM (compressed BAM) files were downloaded from the 1000 Genomes Project FTP (alignment released May 2, 2013). For all 2,508 alignments, we evaluated three genomic positions (chr9: 135,797,259 for *TSC1* c.610C>T; chr9: 135,804,196 for *TSC1* c.64C>T; and chr16: 2,135,300 for *TSC2* c.4639 C>T) to find supporting mutations in normal individuals. For each variant site, only exomes with a read depth greater than or equal to 100 after filtering and a base call quality of Q30 were evaluated. Samples were determined to have a mutation if more than 1% of the reads with more than three of the mutant calls contained the supporting mutations. Our study showed that the identified mutations were negative in 100% of the samples (mutation-positive rate of 0/634 in chr9: 135,797,259; 0/393 in chr9: 135,804,196; and 0/156 in chr16: 2,135,300). To detect copy-number variation (CNV) in panel sequencing data, we utilized the recently developed algorithm copywriteR,[29] which can be applied to sequencing data obtained from target enrichment on small gene panels. This algorithm can extract copy-number information by using uniformly distributed "off-target" sequence reads regardless of the number of genes and target sites. We calculated the number of reads mapping to genome-wide consecutive 100 kb windows (bins) to obtain the depth of coverage. To plot heatmaps of target genes, we processed the "segement.Rdata" file, which was automatically generated by the algorithm with our customized R script.

Droplet Digital PCR for Validating Identified Mutations

The region-specific primers and customized locked nucleic acid (LNA) probes for wild-type and mutant alleles were purchased from Integrated DNA Technology. Detailed sequences of primers and probes are described in Table S10. Genomic DNA extracted from FCD individuals was added to a 20 μL PCR mixture containing 10 μL 2× ddPCR Supermix for Probes (No dUTP, Bio-Rad), 900 nM target-specific PCR primers, and 250 nM mutant-specific (FAM) and wild-type-specific (HEX) LNA probes. 20 μL PCR mixture and 70 μL Droplet Generation Oil for Probes (Bio-Rad) were mixed, and droplets were generated with a QX200 Droplet Generator (Bio-Rad) according to the manufacturer's protocol. The droplet particles were amplified in the following conditions: enzyme activation and denaturation at 95°C for 10 min, 40 cycles of PCR at 94°C for 30 s and 57°C for 2 min, and a final extension and enzyme deactivation at 98°C for 10 min. PCR amplification in droplets was confirmed with the QX200 Droplet Reader (Bio-Rad). Threshold was determined with no-template droplet digital PCR (ddPCR) results. Plots were drawn by the "ddpcr" package in R with raw amplitude data from QuantaSoft.

Site-Specific Amplicon Sequencing

We designed the region-specific primers for validating identified mutations, such as *TSC1* c.64C>T and c.610C>T. In addition, for validation of *Tsc1* and *Tsc2* mutations in mouse brain edited by CRISPR-Cas9 technology, we designed region-specific *Tsc1* and *Tsc2* primers with lengths of 176 and 263 bp, respectively. Target sequences were PCR amplified with PrimeSTAR DNA Polymerase (Takara). For secondary PCR, 20 ng purified PCR product from the first amplification was annealed with both Illumina adaptor and barcode sequences. To verify fragment size and quality of the amplified libraries, we ran individual aliquots on an Agilent 2100 Bioanalyzer. Libraries were pooled and sequenced on an Illumina MiSeq (median read depth of 164,265×).

Mutagenesis for Generating Mutant TSC1 and TSC2 Vectors

pcDNA3.1 Myc-tagged wild-type TSC1 (no. 12133) and pcDNA3 FLAG-tagged wild-type TSC2 (no. 14129) constructs were

purchased from Addgene. These constructs were used for generating TSC1 (GenBank: NM_000368.4) or TSC2 (GenBank: NM_001114382.2) mutant vectors with a QuikChange II Site-Directed Mutagenesis Kit (200523, Stratagene). The primers for mutagenesis were as follows: (1) TSC1 p.Arg22Trp: 5′-GTCACGTCGTCCCACACACCCAGCATG-3′ (sense) and 5′-CATGCTGGGTGTGTGGGACGACGTGAC-3′ (antisense); (2) TSC1 p.Arg204Cys: 5′-CTTTCATACTGTAATGAGAACACAAAAAGGAGACGAAGTTGC-3′ (sense) and 5′-TGCAACTTCGTCTCCTTTTTGTGTTCTCATTACAGTATGAAAG-3′ (antisense); and (3) TSC2 p.Val1547Ile: 5′-TCTCCAACATACAGGATGGCGATCTTGTGGGTG-3′ (sense) and 5′-CACCCACAAGATCGCCATCCTGTATGTTGGAGA-3′ (antisense). After generating mutant constructs, we checked the full sequence of coding region for each construct and found no secondary missense or truncated mutation.

Cell Culture, Transfection, Immunoblotting, and Immunoprecipitation

Human embryonic kidney 293T (HEK293T) and Neuro2A (murine neuroblastoma) cells were cultured in Dulbecco's modified Eagle's medium (DMEM) supplemented with 100 units/mL penicillin, 100 μg/mL streptomycin, and 10% fetal bovine serum at 37°C and 5% CO_2. The cells were transfected with Myc-tagged wild-type and mutant TSC1 and FLAG-tagged wild-type and mutant TSC2 with jetPRIME transfection reagent (Polyplus-transfection). The cells were incubated at 37°C and 5% CO_2 in PBS containing 1 mM $MgCl_2$ and $CaCl_2$. For rapamycin treatment, the cells were co-transfected with HA-S6K vector, Myc-tagged wild-type and mutant TSC1, and FLAG-tagged wild-type and mutant TSC2 and were then treated with 200 nM rapamycin (553210, Calbiochem) for 1 hr. The cells were lysed with PBS containing 1% Triton X-100 and a Halt protease and phosphatase inhibitor cocktail (78440, Thermo Fisher Scientific). Proteins were resolved by SDS-PAGE and transferred to polyvinylidene difluoride (PVDF) membranes (Millipore). The membranes were blocked with 3% BSA in Tris-buffered saline (TBS) containing 0.1% Tween 20 (TBST) for 1 hr at room temperature. They were washed four times with TBST. The membranes were incubated with primary antibodies including a 1/1,000 dilution of anti-phospho-S6 ribosomal protein (5364, Cell Signaling Technology), anti-S6 ribosomal protein (2217, Cell Signaling Technology), anti-phopho-p70 S6 kinase (Thr389; 9205, Cell Signaling Technology), anti-p70 S6 kinase (9202, Cell Signaling Technology), anti-FLAG M2 (8146, Cell Signaling Technology), α-tubulin (T6074, Sigma-Aldrich), anti-Myc (2276, Cell Signaling Technology), anti-TSC1 (6935, Cell Signaling Technology), and anti-TSC2 (3990, Cell Signaling Technology) in TBST overnight at 4°C. After incubation, the membranes were washed four times with TBST. They were incubated with a 1/5,000 dilution of horseradish-peroxidase-linked anti-rabbit or anti-mouse secondary antibodies (7074, Cell Signaling Technology) for 2 hr at room temperature. For immunoprecipitation, lysates were immunoprecipitated with anti-TSC2 (3990, Cell Signaling Technology) or anti-Myc (2276, Cell Signaling Technology) antibody overnight. This mixture was incubated with protein A+G magnetic beads for 2 hr. After protein A agarose beads were washed three times with PBS containing 1% Triton X-100, the beads were incubated with SDS sample buffer at 37°C for 10 min. The eluted proteins were resolved on SDS-PAGE gel and transferred to a PVDF membrane. Immunoblotting was performed as described above.

GTP-Agarose Pull-Down Assay

Cells were harvested in lysis buffer (20 mM Tris-HCl [pH 7.5], 5 mM $MgCl_2$, 2 mM PMSF, 20 μg/mL leupeptin, 10 μg/mL aprotinin, 150 mM NaCl, and 0.1% Triton X-100) and then lysed by sonication for 15 s. Cell lysates were centrifuged at 13,000 × *g* for 10 min at 4°C, and the supernatant was collected. The supernatant was incubated with 100 μL GTP-agarose beads (G9768, Sigma-Aldrich) in 500 μL lysis buffer for 30 min at 4°C. The beads were washed with lysis buffer, and the supernatant was retained. The retained supernatant was incubated with washed beads for another 30 min. The beads were washed again and then incubated with the retained supernatant overnight at 4°C. After being washed five times with lysis buffer, GTP-bound protein extracts were eluted, and the GTP-bound proteins were visualized by immunoblot analysis.

Immunohistochemistry in Pathological Samples

Non-MCD (malformation of cortical development) brain specimen was collected in the operating room from the tumor-free margin of an individual with glioblastoma as part of a planned resection and was pathologically confirmed to be normal brain tissue without a tumor. Surgical tissue blocks were fixed in freshly prepared phosphate-buffered 4% paraformaldehyde (PFA) overnight, cryoprotected overnight in 20% buffered sucrose, and made into gelatin-embedded tissue blocks (7.5% gelatin in 10% sucrose and phosphate buffer [PB]), which were stored at −80°C. Cryostat-cut sections (10 μm thick) were collected and placed on glass slides. FFPE slides were deparaffinized and rehydrated for the removal of paraffin. Then, deparaffinized FFPE slides were used in a heat-induced retrieval process with citrate buffer (sodium citrate 10 mM [pH 6.0]) for enhancing the staining intensity of antibodies. Cryostat-cut sections or processed FFPE slides were blocked in PBS-GT (0.2% gelatin and 0.2% Triton X-100 in PBS) for 1 hr at room temperature and stained with the following antibodies: rabbit antibody to phosphorylated S6 ribosomal protein (Ser240/Ser244, 1:100 dilution; 5364, Cell Signaling Technology) and mouse antibody to NeuN (1:100 dilution; MAB377, Millipore). Samples were then washed in PBS and stained with the following secondary antibodies: Alexa Fluor 488-conjugated goat antibody to mouse (1:200 dilution; A21422, Invitrogen) and Alexa Fluor 555-conjugated goat antibody to rabbit (1:200 dilution; A11008, Invitrogen). DAPI included in mounting solution (P36931, Life Technologies) was used for nuclear staining. We acquired images by using a Zeiss LSM780 confocal microscope (Carl Zeiss). The number of cells positive for NeuN was determined with the 10× objective lens; 3~4 fields were acquired per subject within the neuron-rich region. The number of DAPI-positive cells represents the total cell count. Neuronal cell size was measured in NeuN-positive cells according to the automated counting protocol of ImageJ software.

Cloning the CRISPR Construct

The hSpCas9 nuclease-expressing pX330 plasmid (no. 42230)[30] was purchased from Addgene. Using the QuikChange Site-Directed Mutagenesis Kit (Stratagene), we modified the sgRNA cloning sites of pX330 by changing the BbsI recognition site (GAAGAC) to that of BsaI (GGTCTC). To generate U6-sgRNA-Cas9-IRES-mCherry plasmids, we PCR amplified IRES-mCherry with IRES3-mCherry-CL plasmids (kindly provided by Prof. Chang Hwan Park of Hanyang University) as a template and inserted it between the Cas9 sequence and the 3′ nuclear localization sequence of pX330. To screen sgRNAs and generate knockout clones, we used a plasmid encoding Cas9-2A-mRFP-2A-PAC

(puromycin *N*-acetyl-transferase, puromycin resistance gene) and a plasmid encoding sgRNAs (both from ToolGen). The sgRNA target sequences were manually designed on the basis of the protospacer adjacent motif (PAM) sequence (NGG) and cloned into the vectors as previously described.[31] In brief, oligonucleotides containing each target sequence were synthesized (Bioneer) and annealed in vitro with a thermocycler. The vector was digested with BsaI and ligated with the annealed oligonucleotides. Oligonucleotide sequences are listed in Table S7.

Screening of sgRNAs Targeting *TSC1* and *TSC2*

Neuro2A cells were co-transfected with plasmids encoding Cas9 and sgRNA targeting the *TSC1* or *TSC2* locus at a 1:2 weight ratio with polyethyleneimine (PEI; linear, molecular weight ~ 25,000; Polysciences) or Neon (Invitrogen), respectively, according to the manufacturers' instructions. 1 day after transfection, cells were subjected to puromycin selection (1 μg/mL) for 2 days, after which cells were subjected to the T7E1 assay.

T7E1 Assay

The T7E1 assay was performed as previously described.[32,33] Genomic DNA was isolated with the Wizard Genomic DNA Purification Kit (Promega) according to the manufacturer's instructions. The region including the nuclease target site was amplified by nested PCR with the appropriate primers (Table S8). The amplicons were denatured by heating and annealed to allow the formation of heteroduplex DNA, which was treated with 5 units of T7 endonuclease 1 (New England Biolabs) for 20 min at 37°C and then analyzed by 2% agarose gel electrophoresis. Mutation frequencies were calculated as previously described on the basis of the band intensities with ImageJ software and the following equation:[34] mutation frequency (%) = 100 × (1 − (1 − fraction cleaved)$^{1/2}$), where the fraction cleaved is the total relative density of the cleavage bands divided by the sum of the relative density of the cleavage bands and uncut bands.

Generation of Knockout Clones

Neuro2A cells were co-transfected with plasmids encoding Cas9 and sgRNA targeting the *Tsc1* or *Tsc2* locus at a 1:2 weight ratio with PEI or Neon, respectively. 1 day after transfection, cells were subjected to puromycin selection (1 μg/mL) for 3 days. Then, cells were trypsinized and resuspended in DMEM and seeded into 96-well plates at an average density of 0.25 cells/well. 20 days after cell seeding, each well was microscopically evaluated, and single-cell-derived round colonies were selected.[31] Each selected colony was individually trypsinized and re-plated into 24-well plates. 6 days after the subculture, genomic DNA was isolated from each clone and subjected to the T7E1 assay and sequencing as described above.

Sanger Sequencing of Selected Clones

Sequencing of the genomic region including the target sequence was performed as previously described.[35] In brief, PCR amplicons that included nuclease target sites were cloned into the T-Blunt vector (Promega), and the cloned plasmids were sequenced with the M13 forward primer (5′-GTAAAACGACGGCCAGT-3′).

Cas9 Nickase and Nuclease Plasmids, Single-Stranded Oligodeoxynucleotides, and Transfection

We obtained a plasmid encoding Cas9-2A-mRFP-2A-PAC for nuclease and a plasmid encoding sgRNAs from ToolGen. We purchased a Cas9-nickase-encoding vector from Addgene (no. 51130). 102-mer single-stranded oligodeoxynucleotide (ssODN) templates, purchased from IDT, were designed to contain silent mutations with restriction enzyme sites (Figure S16A). Modified ssODNs contained phosphorothioate bases at the terminal three positions of the 5′ and 3′ ends.[36] The ssODNs were diluted with RNase-free water to 100 μM, divided into aliquots, and stored at −20°C. Neuro2a cells at 90% confluence in 6-well plates were co-transfected with 12–15 μg plasmids encoding Cas9 nuclease or nickase, a plasmid encoding single guide RNA (sgRNA), and ssODNs at a 1:2:9 or 2:4:9 weight ratio with Lipofectamine 2000 (Life Technologies) according to the manufacturer's instructions. Genomic DNA was isolated from transfected cells with the Wizard Genomic DNA Purification Kit (Promega) 3 days after transfection by a restriction fragment length polymorphism (RFLP) assay and deep sequencing.

RFLP Assay and Deep Sequencing

Genomic DNA was PCR amplified, and 10 μL of PCR amplicons was digested with 1 unit of NdeI (NEB) at 37°C in a total reaction volume of 30 μL. After 3 hr of digestion, the product was analyzed by 2% agarose gel electrophoresis. RFLP frequencies were calculated as previously described on the basis of the band intensities with ImageJ software and the following equation:[34] mutation frequency (%) = 100 × (1 − (1 − fraction cleaved)$^{1/2}$), where the fraction cleaved is the total relative density of the cleavage bands divided by the sum of the relative density of the cleavage bands and uncut bands. For deep sequencing, target sequences were PCR amplified with phusion polymerase (NEB). For secondary PCR, 20 ng purified PCR product from the first amplification was annealed with both adaptor and barcode sequences (Illumina). The primers used for the PCR reactions are shown in Table S9. The resulting products were column purified and analyzed with an Illumina HiSeq at Macrogen.

In Utero Electroporation and Image Analysis

Timed pregnant mice (embryonic day [E] 14) were anesthetized with isoflurane (0.4 L/min of oxygen and isoflurane vaporizer gauge 3 during surgery). The uterine horns were exposed, and a lateral ventricle of each embryo was injected via pulled glass capillaries with 2 μg/mL Fast Green (F7252, Sigma) combined with 2–3 mg appropriate plasmids as indicated. For generation of the seizure mouse model with a CRISPR-Cas9 construct expressing sgRNA targeting *Tsc1* or *Tsc2*, wild-type embryos were co-transfected with a CRISPR-Cas9-mcherry vector (with or without sgRNA) and pCAG-dsRed plasmids. Because the intensity of mcherry signal is not sufficient for screening the plasmid-expressing pups while alive via external fluorescence excitation, pCAG-dsRed plasmid was used for enhancing red signal. To induce homology-directed repair (HDR)-mediated genome editing without indels, we transfected the embryos with plasmids encoding Cas9 nickase (Cas9n), plasmids encoding sgRNA, and ssODNs at a 1:2:20 DNA molar ratio. We electroporated the plasmids on the head of the embryo by discharging 50 V with the ECM830 electroporator (BTX-Harvard Apparatus) in five electric pulses of 100 ms at 900 ms intervals. Embryonic mice were electroporated at E14, and then mouse pups that expressed the red fluorescence signal were selected at birth (postnatal day [P] 0) for subsequent analysis. Their brains were harvested after >56 days of development (P56) by perfusion fixation with 4% freshly prepared phosphate-buffered PFA solution and were additionally fixed in freshly prepared

phosphate-buffered 4% PFA overnight. Then, fixated mouse brains were cryoprotected overnight in 30% buffered sucrose and made into gelatin-embedded tissue blocks (7.5% gelatin in 10% sucrose and PB), which were stored at −80°C. Cryostat-cut sections (20 μm thick) were collected and placed on glass slides. DAPI included in mounting solution (P36931, Life Technologies) was used for nuclear staining. We acquired images with a Zeiss LSM780 confocal microscope. Cortical layers were identified with DAPI counterstaining and distinguished with anatomical landmarks (e.g., callosum and marginal zone) and cell density. Each layer of the affected cortical region was divided into a region of interest. Fluorescence intensities reflecting the distribution of electroporated cells within the cortex were converted into gray values and measured from layer V/VI to layer II/III with ImageJ software. The number of DAPI-positive cells represents the total cell count, which we used to measure the percentage of dsRed-positive cells. To measure cell size, we determined the number of cells positive for NeuN by using the 20× objective lens. Neuronal cell size was measured in NeuN-positive cells according to the automated counting protocol of ImageJ software.

Laser Capture Microdissection

Adult mouse brain samples were fixed in freshly prepared phosphate-buffered 4% PFA overnight, cryoprotected overnight in 30% buffered sucrose, and made into gelatin-embedded tissue blocks (7.5% gelatin in 10% sucrose and PB), which were stored at −80°C. Cryostat-cut sections (10 μm thick) were collected and placed on glass slides. After DAPI staining, dsRed-positive neurons in mouse brain (n = ~20 per case) were microdissected with the PALM laser capture system (Carl Zeiss) and collected in AdhesiveCap (Carl Zeiss). Genomic DNA was extracted from the collected neurons according to the laser capture microdissection (LCM) protocol of the QIAamp DNS Micro Kit (QIAGEN). Genomic DNA extracted from dissected neuron was subjected to site-specific amplicon sequencing.

In Vivo Rapamycin Treatment

Mice were treated with rapamycin as previously described.[37] In brief, rapamycin (LC Labs) was dissolved initially in 100% ethanol to 20 mg/mL stock solution, stored at 20°C. Immediately before injection, stock solution was diluted in 5% polyethyleneglycol 400 and 5% Tween 80 to final concentrations of 1 mg/mL rapamycin and 4% ethanol. Mice were injected daily through an intraperitoneal route with 10 mg/kg rapamycin or vehicle alone for 2 weeks.

Video-EEG Monitoring

EEG signals from the epidural electrodes located on the frontal lobes (anterioposterior [AP], +2.8 mm; mediolateral [ML], ±1.5 mm) and temporal lobes (AP, −2.4 mm; ML, ±2.4 mm) were recorded with the cerebellum as a reference. After >4 days of recovery from the surgery, EEG signals were recorded for >2 days (12 hr/day). Signals were amplified with an RHD2000 Amplifier Chip (Intan Technologies), recorded with an RHD2000 USB Interface Board (Intan Technologies), and analyzed with open-source MATLAB toolbox EEGLAB.

Statistical Analyses

All values in figures are presented as the mean ± SEM. Results were analyzed with Student's t test or ANOVA where appropriate with GraphPad Prism 6 (GraphPad Software). A Bonferroni post hoc test was used for analyzing significant differences in the ANOVA test. A p value less than 0.05 was considered statistically significant.

Results

Identification of Brain Somatic Mutations in *TSC1* and *TSC2* from FCDII Individuals Lacking *MTOR* Mutations

To examine brain somatic mutations in upstream regulators of mTOR kinase, we first performed targeted deep sequencing of five mTOR pathway genes (*PIK3CA*, *PIK3R2*, *AKT3*, *TSC1*, and *TSC2*) in FFPE brain samples obtained from 40 FCDII individuals who had been previously found to be negative for *MTOR* mutations[8] (Table S1). Two orthogonal sequencing platforms were used: hybrid capture (read depth of 100×–17,556×) and PCR-based amplicon sequencing (read depth of 100×–20,012×) (Figure S2). We used hybrid capture sequencing data followed by Genome Analysis Toolkit (GATK) analysis to screen germline mutations in five mTOR pathway genes. No pathogenic germline mutations were found in the studied individuals (Figure S2). Next, somatic single-nucleotide variants and indels were designated with an in-house script and the Strelka algorithm,[38] respectively. To minimize erroneous and false-positive mutations that could mimic low-level somatic mutations, we performed cross-platform replications by adopting both hybrid capture and PCR-based amplicon sequencing of five genes.[8,39,40] To detect true de novo somatic mutations, we selected overlapping mutations in both sequencing platforms and then performed simple filtering steps (Figure S2). The subjects were considered to have a mutation when the percentage of mutated reads exceeded 10× (1%) the expected base miscall rate (0.1%).[28] In addition, we performed additional confirmatory tests such as ddPCR or ultra-high depth (>100,000×) site-specific amplicon sequencing to further validate the candidate somatic mutations (Figure S3). As a result, our analysis revealed three missense mutations in *TSC1* (GenBank: NM_000368.4) and *TSC2* (GenBank: NM_000548.4)—*TSC1* c.64C>T (p.Arg22Trp), *TSC1* c.610C>T (p.Arg204Cys), and *TSC2* c.4639G>A (p.Val1547Ile)—which were found in 5 of 40 (12.5%) FCDII individuals negative for *MTOR* mutations (Figure 1B and Tables 1 and S1). In these five individuals with *TSC1* or *TSC2* somatic mutations, we could not detect any abnormal clinical findings related to TSC under the guidance of surveillance recommendations for suspected TSC[27] (Table S2). We also examined the possibility of germline CNV of *TSC1* or *TSC2* in these five individuals. To detect germline CNV in targeted sequencing data, we utilized the recently developed algorithm of CNV detection, which can be applied to sequencing data obtained from target enrichment on small gene panels.[29] As a result, we could not find any germline CNV in these individuals, suggesting that CNV is not implicated in these individuals with *TSC1* or *TSC2* somatic mutations (Figure S4A). The identified mutations were not detected in the available

Table 1. Clinical and Molecular Data from FCDII-Affected Individuals Harboring *TSC1* and *TSC2* Mutations

Individual	Age at Surgery	Sex	Pathology	MRI Report	Protein	Nucleotide Change	Protein Change	% Mutated Allele	
								Hybrid Capture	PCR Amplicon Sequencing
FCD 64	6 years, 9 months	female	cortical dyslamination and dysmorphic neurons (consistent with FCDIIa)	cortical dysplasia involving the left frontoparietal lobe	TSC1	c.610C>T	p.Arg204Cys	1.75%	1.0%
FCD 81	12 years	female	cortical dyslamination and dysmorphic neurons (consistent with FCDIIa)	no abnormal signal intensity	TSC1	c.64C>T	p.Arg22Trp	2.81%	2.0%
FCD 94	10 years, 3 months	female	cortical dyslamination and dysmorphic neurons (consistent with FCDIIa)	subependymal heterotopia in the right peri-trigone area	TSC2	c.4639G>A	p.Val1547Ile	1.19%	1.55%
FCD 98	14 years, 3 months	male	cortical dyslamination and dysmorphic neurons (consistent with FCDIIa)	no abnormal signal intensity	TSC1	c.64C>T	p.Arg22Trp	2.52%	1.98%
FCD 123	12 years, 4 months	female	cortical dyslamination, dysmorphic neurons, and balloon cells (consistent with FCDIIb)	cortical dysplasia involving the right frontal lobe	TSC1	c.64C>T	p.Arg22Trp	2.21%	1.37%

saliva samples from mutation-positive individuals (Table S3), nor were they detected in 100% of the exomes from 1000 Genomes according to the same filtering criteria that were applied in our analysis (>100× read depth and four mutant calls). In addition, we checked the allele frequency of these three mutations in the Exome Aggregate Consortium (ExAC) Browser and found that the minor allele frequencies (MAFs) of *TSC1* c.64C>T and *TSC2* c.4639G>A were 1.65×10^{-5} and 3.34×10^{-5}, respectively. The *TSC1* c.610C>T mutation was not found in the ExAC Browser. Because these identified mutations exist as very rare variants in the ExAC Browser, it is unlikely that they are non-pathogenic and common mutations. Interestingly, among these three mutations, *TSC1* c.64C>T was detected recurrently in three individuals (Table 1). The *TSC1* c.64C>T variant has recently been reported in a case of nasopharyngeal carcinoma without functional analysis.[41] The allelic frequencies of the detected mutations ranged from 1.0% to 2.8% (Tables 1, S4, and S5). In addition, three amino acid positions affected by the identified mutations were found to be evolutionarily conserved (Figure 1C and Table S6).

Identified *TSC1* and *TSC2* Mutations Lead to Aberrant Activation of the mTOR Pathway

TSC1 (encoding hamartin) and *TSC2* (encoding tuberin) are tumor-suppressor genes in which most germline mutations are identified in TSC. TSC is an autosomal-dominant multisystem disorder characterized by hamartomas in multiple organ systems, including the brain, kidney, skin, heart, and lung.[18] None of the identified mutations in *TSC1* and *TSC2* have been reported in the LOVD Tuberculosis Sclerosis Database. TSC1 and TSC2 directly interact with one another and form the heterodimeric TSC complex, which plays a critical role in negatively regulating mTOR kinase via its GTPase-activating protein (GAP) activity toward Ras homolog enriched in brain (Rheb) (Figure 2A). TSC1 is required to stabilize TSC2 as the TSC1-TSC2 complex and the GAP domain on TSC2 hydrolyze Rheb-GTP to Rheb-GDP, thereby inhibiting the activation of mTOR kinase[42] (Figure 2A). Several studies have reported that various genetic mutations in *TSC1* or *TSC2* can disrupt the formation or function of the TSC complex and result in aberrant activation of mTOR kinase.[43–45] In addition, heterozygous germline missense mutations or haploinsufficiency of *TSC1* or *TSC2* is sufficient to cause hyperactivation of the mTOR pathway and various symptoms of TSC, including epilepsy.[37,46–48] Therefore, it is likely that the identified somatic mutations induce hyperactivation of the mTOR pathway by affecting the formation or function of the TSC complex.

To test this possibility, we transiently co-transfected human HEK293T with wild-type or mutant Myc-tagged TSC1 and FLAG-tagged TSC2. Next, we performed immunoblot analysis to assess the phosphorylation of S6 kinase (S6K), which is a major readout of mTOR activation.[49,50] Compared with wild-type *TSC1*- and *TSC2*-expressing

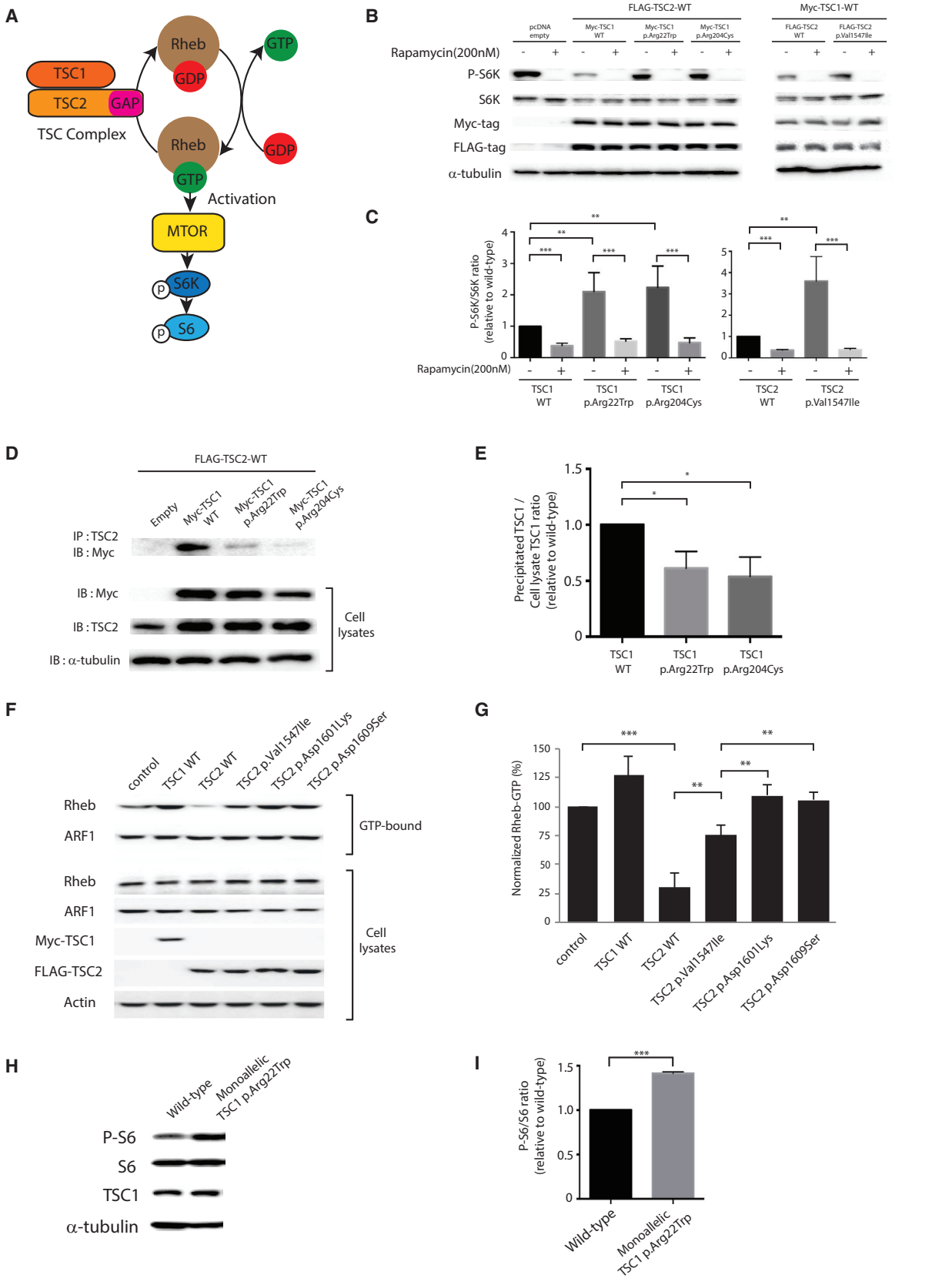

Figure 2. The Identified Mutations Induce Hyperactivation of the mTOR Pathway by Disrupting the Formation or Function of the TSC1-TSC2 Complex

(A) Schematic figure showing that mTOR kinase activation is regulated by the GAP domain of the TSC complex through hydrolysis of GTP-bound Rheb.

(legend continued on next page)

cells, mutant *TSC1*- and *TSC2*-expressing cells failed to inhibit phosphorylation of S6K (Figures 2B and 2C). In addition, we found that phosphorylation of S6K in mutant *TSC1*- or *TSC2*-expressing cells was inhibited by treatment with rapamycin (an mTOR inhibitor) (Figures 2B and 2C). This result indicates that the TSC complex's ability to inhibit the activation of mTOR kinase was compromised in these mutant cells. Next, to examine the molecular mechanism underlying the effects of these mutations on the TSC complex, we first tested whether mutations in *TSC1* and *TSC2* disrupt the formation of the TSC1-TSC2 complex by performing co-immunoprecipitation assays in HEK293T cells expressing wild-type and mutant TSC1 or TSC2. We found that TSC1 p.Arg22Trp and p.Arg204Cys profoundly inhibited TSC1 binding to TSC2 (Figures 2D and 2E). Interestingly, TSC1 p.Arg204Cys slightly reduced the stability of TSC1. However, TSC2 p.Val1547Ile did not affect TSC2 binding to TSC1 (Figures S5A and S5B). These data suggest that TSC1 p.Arg22Trp and p.Arg204Cys, but not TSC2 p.Val1547Ile, disrupt the proper formation of the TSC1-TSC2 complex. Considering that TSC2 p.Val1547Ile is located in the GAP domain of TSC2, this variant is likely to affect the GAP activity of the TSC1-TSC2 complex toward Rheb but not the formation of the TSC1-TSC2 complex (Figures 1B and 2A). To test this possibility, we performed GTP-agarose pull-down assays and measured the levels of GTP-bound Rheb in cells expressing wild-type and mutant TSC2. We compared the levels of GTP-bound Rheb between TSC2-p.Val1547Ile-expressing cells and wild-type cells or cells expressing two known enzyme-dead point substitutions (TSC2 p.Asn1601Lys and p.Asn1609Ser).[45] Although TSC2 p.Val1547Ile did not completely abolish GAP activity, GTP-bound Rheb levels were robustly higher in cells expressing TSC2 p.Val1547Ile than in cells with wild-type TSC2, suggesting that TSC2 p.Val1547Ile strongly inactivated GAP activity without affecting the levels of the unrelated GTP-bound protein, ARF1 (Figures 2F and 2G). This finding suggests that TSC2 p.Val1547Ile strongly inhibited the GTPase activity of the TSC complex and thereby led to a loss of function of the TSC complex.

Furthermore, to test whether the somatic heterozygous mutation could induce hyperactivation of the mTOR pathway, we modeled the monoallelic *TSC1* c.64C>T (p.Arg22Trp) substitution that was recurrently found in three individuals by using HDR-mediated genome editing with the CRISPR-Cas9 system. We generated a Neuro2A cell line carrying monoallelic *TSC1* c.64C>T mutations (Figure S6). We found that the phosphorylation of S6 was significantly increased in mutated cells without affecting the level of TSC1, indicating that the somatic heterozygous mutation induces hyperactivation of the mTOR pathway (Figures 2H and 2I). Together, all of these findings indicate that our identified mutations disturb either the formation or the function of the TSC1-TSC2 complex and thereby lead to hyperactivation of mTOR kinase via loss of function of the TSC complex.

The Identified Mutations Are Associated with Aberrant mTOR Activation and Dysmorphic Neurons in Brain Tissues of Individuals with FCD

Next, to determine whether the affected brains of FCDII individuals carrying *TSC1* or *TSC2* mutations were associated with aberrant mTOR activation, we performed co-immunostaining to detect S6 phosphorylation (P-S6) and NeuN, a neuronal marker, in FFPE sections obtained from FCDII individuals carrying mutations (Figure 3A). The results revealed a robustly higher number of P-S6-positive neuronal cells in individuals carrying *TSC1* and *TSC2* somatic mutations than in non-FCD brains (Figures 3A and 3B). In addition, we measured the cell sizes of P-S6-positive neurons and observed a robust increase in the soma size in

(B) Immunoblot analysis of S6K phosphorylation in *TSC1* or *TSC2* mutant HEK293T cells. HEK293T cells were transiently transfected with Myc-tagged wild-type *TSC1* and the indicated *TSC1* mutants or with FLAG-tagged wild-type *TSC2* and the indicated *TSC2* mutant and then treated with rapamycin (200 nM) for 1 hr. Cell lysates were subjected to immunoblot analysis with the indicated antibodies. WT, wild-type.
(C) Quantification of the blotting intensity. Data represent the mean ± SEM (n = 3–5 per group). **$p < 0.01$ and ***$p < 0.001$ compared with the wild-type (Student's t test).
(D) Immunoprecipitation assay of mutant TSC1 and wild-type TSC2. HEK293T cells were transiently co-transfected with Myc-tagged wild-type or mutant TSC1 and FLAG-tagged wild-type TSC2. Lysates were immunoprecipitated with anti-TSC2 antibody and subsequently immunoblotted with anti-Myc antibody. Immunoprecipitation assays of mutant TSC2 and wild-type TSC1 are presented in Figure S5.
(E) Quantification of the TSC1 blotting intensity immunoprecipitated with TSC2 antibody. Data represent the mean ± SEM (n = 4 per group). *$p < 0.05$ compared with the wild-type (Student's t test).
(F) GTP-agarose bead pull-down assay for Rheb in mutant *TSC2*-expressing cells. HEK293 cells were transfected or co-transfected with Myc-tagged wild-type TSC1, FLAG-tagged wild-type TSC2, or TSC2 p.Val1547Ile. Cell lysates were incubated with GTP-agarose beads, and the GTP-bound materials were analyzed by immunoblotting with anti-Rheb or anti-ARF1 antibodies. Total cell lysates were also immunoblotted with the indicated antibodies.
(G) Quantification of the GTP-bound Rheb blotting intensity. Two point substitutions (TSC2 p.Asn1601Lys and p.Asn1609Ser) have been reported to abolish TSC2 GAP activity and thus were used as the enzyme-dead control. Data represent the mean ± SEM (n = 3 per group). **$p < 0.01$ and ***$p < 0.001$ (Student's t test).
(H) Immunoblot analysis of phosphorylated S6 (P-S6), S6, and Tsc1 in Neuro2A cells carrying monoallelic TSC1 p.Arg22Trp. The level of phosphorylated S6 was significantly increased in the stable cell line with monoallelic TSC1 p.Arg22Trp, indicating that the mTOR pathway was hyperactivated by the heterozygous monoallelic mutation. The level of TSC1 was unaffected by the mutation.
(I) Quantification of the blotting intensity of S6 phosphorylation. Data represent the mean ± SEM (n = 3 per group). ***$p < 0.001$ compared with the wild-type (Student's t test). Cells were harvested without serum starvation for lysate extraction in all experiments.

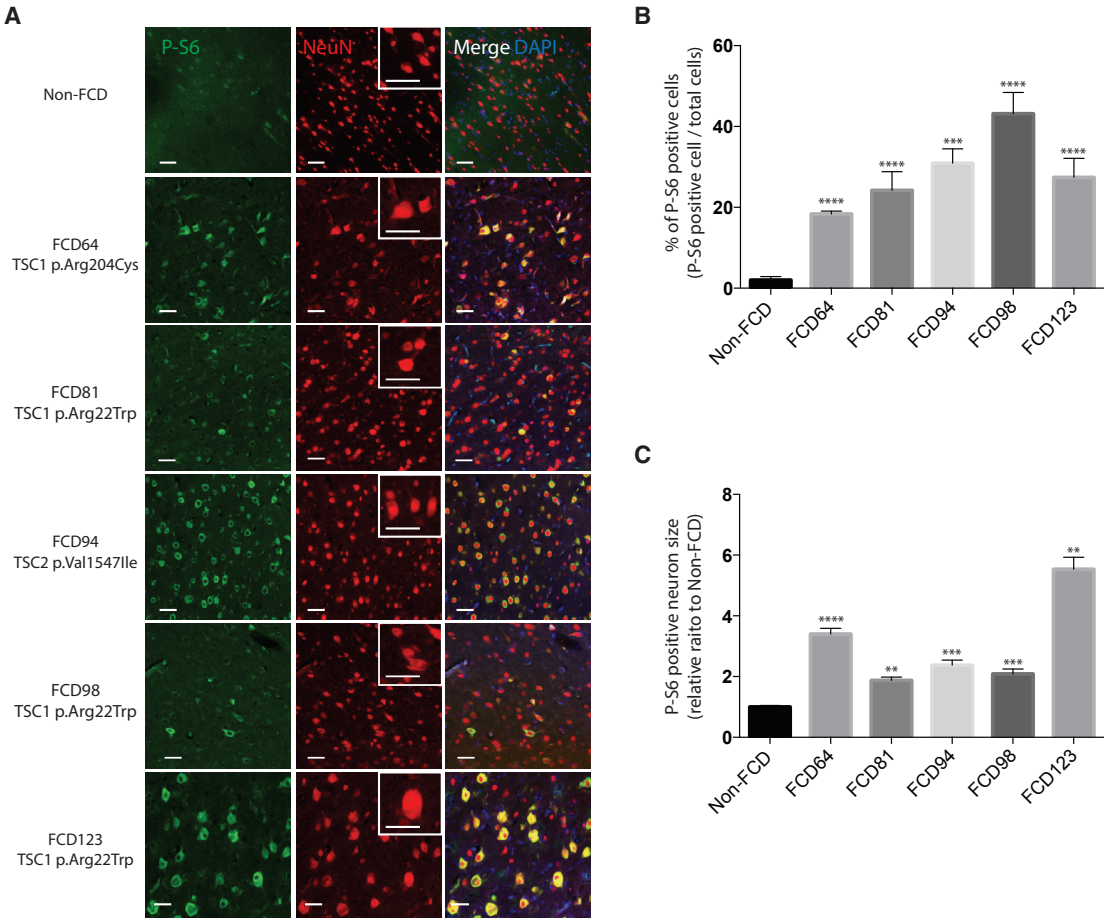

Figure 3. The Identified Mutations Are Associated with Aberrant mTOR Activation and Cytomegalic Neurons in Individuals with FCDII

(A) Co-immunostaining of pathological samples obtained from FCDII individuals carrying *TSC1* or *TSC2* mutations for the mTOR pathway marker P-S6, the neuronal marker NeuN, and DAPI. Non-FCD brain specimens were collected from the tumor-free margin of an individual with glioblastoma as part of a planned resection, which was pathologically confirmed as normal brain tissue without a tumor. The percentage of P-S6-positive cells and the soma size of P-S6-positive neuronal cells were measured. Scale bars, 50 μm.

(B and C) The bar chart shows the percentage of P-S6-positive cells (B) and the soma size of P-S6-positive neurons (C). The bar charts correspond to an average of three to four representative cortical regions. Data represent the mean ± SEM (n = 39–134 per group). **p < 0.01, ***p < 0.001, and ****p < 0.0001 compared with the non-FCD sample (Student's t test).

the pathological samples (Figures 3A and 3C). These results suggest that the identified *TSC1* and *TSC2* mutations are closely associated with both aberrant mTOR activation and dysregulation of neuronal growth in individuals with FCDII.

In Utero Application of the CRISPR-Cas9 System Models Somatic Loss-of-Function Mutations in the TSC Complex

We further examined whether such a small fraction (e.g., 1.0%–2.8% of the mutated allele frequency) of neurons with defective TSC1-TSC2 complex function were sufficient to cause behavioral seizures, as well as the cortical dyslamination and cytomegalic neurons observed in individuals with FCDII. It is known that both biallelic and monoallelic indels in *TSC1* or *TSC2* cause mTOR pathway hyperactivation by disturbing the function of the TSC complex.[22,51,52] Thus, to mimic the disrupted function observed in individuals, we attempted in utero application of the CRISPR-Cas9 system to introduce indels into *Tsc1* or *Tsc2* via non-homologous end joining (NHEJ) in focal cortical regions of the developing mouse brain. To achieve this goal, we first designed sgRNAs targeting exon 3 of *Tsc1* and exon 2 of *Tsc2* (Figures S7A and S7B) and then selected proper sgRNAs to induce indels with an efficacy of 52%–60% for *Tsc1* and 44%–65% for *Tsc2* with the T7E1 assay (Figures S7C and S7D). Next, to test whether our selected sgRNAs with Cas9 targeting *Tsc1* or *Tsc2* led to hyperactivation of the mTOR pathway, we generated biallelic *Tsc1*- or *Tsc2*-mutated Neuro2A clones (Figure S8) and performed immunoblot analysis to detect P-S6, TSC1, and TSC2. We found that TSC1 and TSC2 were knocked out and that the level of P-S6 was robustly increased in both mutated cell lines, indicating that TSC complex disruption resulted in hyperactivation of the mTOR pathway (Figure S9). Next, we performed in utero electroporation of the selected sgRNAs expressing the CRISPR-Cas9

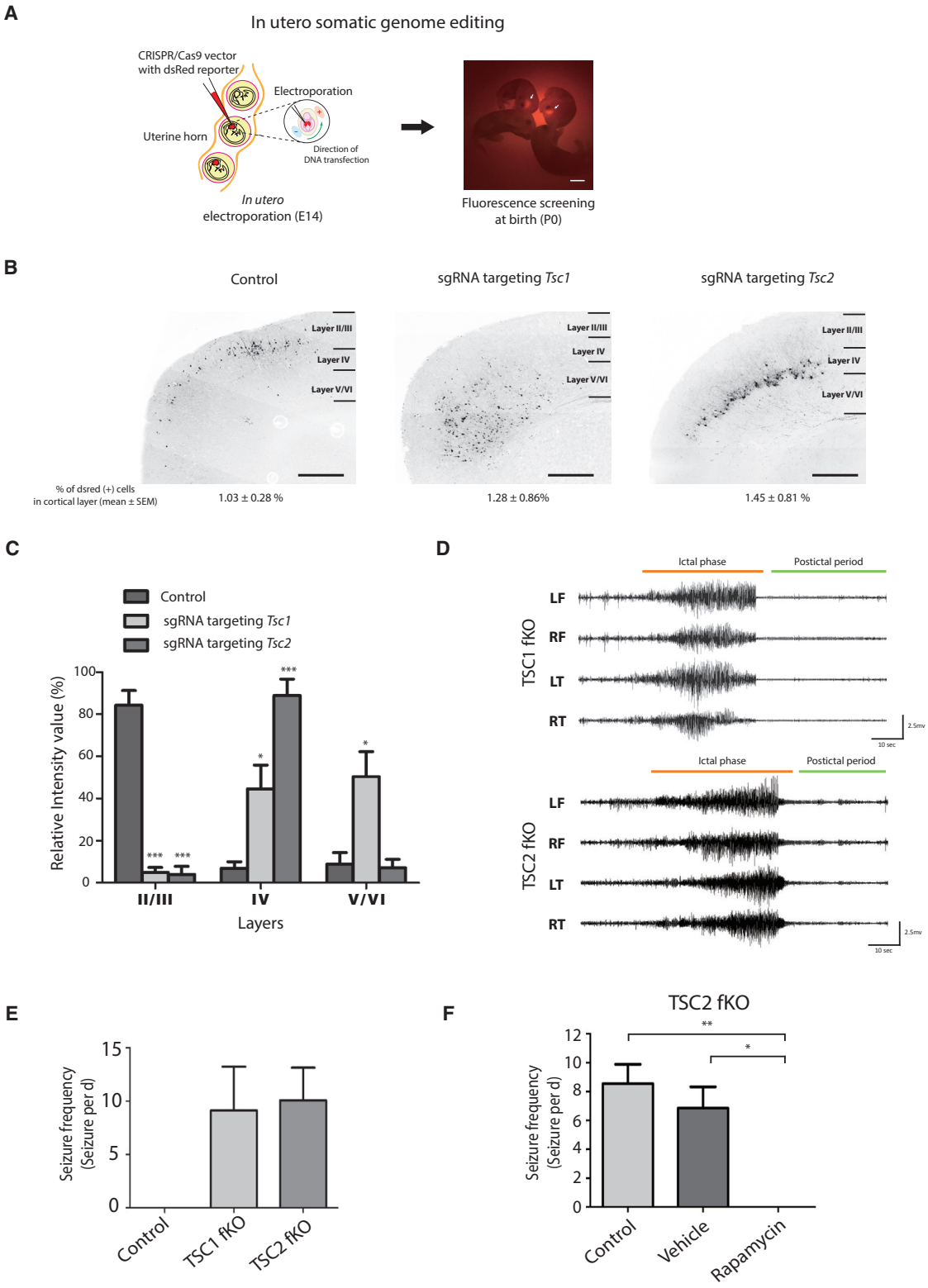

Figure 4. In Utero Somatic Genome Editing of *Tsc1* and *Tsc2* Recapitulates the Pathology and Symptoms Observed in Individuals with FCDII

(A) Schematic figure of the procedure used to generate the mouse model of brain somatic mutations induced by in utero somatic genome editing in the developing brain. In utero electroporation of CRISPR-Cas9 vectors with a dsRed reporter targeting *Tsc1* or *Tsc2* was performed at E14, and properly electroporated and delivered mice were screened at birth (P0). Then, they were monitored by video-electroencephalography (EEG) after 3 weeks of age. The arrow indicates the focal expression of the dsRed reporter in the embryonic mouse brain. Scale bar, 3 mm.

(legend continued on next page)

vector in the developing mouse brain to examine whether a focal disruption of the *Tsc1* or *Tsc2* focal knockout (fKO) caused the FCDII phenotypes. We electroporated *Tsc1*- or *Tsc2*-targeted CRISPR-Cas9 constructs (sgRNA-Cas9-IRES-mCherry vector) with a dsRed reporter vector (pCAG-dsRed) into the developing mouse brain on E14 and measured the percentage of dsRed-positive neurons after P56 (Figures 4A and S10). We found that mouse brain regions electroporated with Cas9 and sgRNA contained 1.03%–1.45% dsRed-positive cells. These percentages are similar to the mutational burdens observed in individuals with FCDII (Figure 4B). We further examined whether our CRISPR-Cas9 system could significantly reduce the level of target protein within the time frame of neuronal development in the early embryonic mouse brain. After in utero electroporation of *Tsc2*-targeted CRISPR-Cas9 constructs with a dsRed reporter vector at E14, we examined the migration of the dsRed-positive neurons and the level of TSC2 at E18 (Figure S10). We found that the number of dsRed-positive cells electroporated with the CRISPR construct targeting *Tsc2* was significantly lower in the cortical plate (CP) and higher in the intermediate zone (IZ) and subventricular zone (SVZ) than in the control group. This result indicates that radial migration of the cortical neurons was abrogated in the developing mouse brain (Figure S11A and S11B). In addition, to measure the level of TSC2 targeted by CRISPR in the migration window, we dissected the dsRed-positive region from the electroporated embryonic brain at E18 to enrich the genome-edited cells (Figure S11C). Next, we extracted the protein lysate for subsequent immunoblot analysis. The results showed that the TSC2 level targeted by CRISPR was significantly decreased by ~40% (Figure S11D and S11E) in the focal cortical region of the embryonic brain. Moreover, to demonstrate the increased P-S6 in these brain tissues, we performed immunohistochemistry staining in embryonic mouse brain sections electroporated with the CRISPR construct. The result showed that cells expressing the CRISPR construct targeting *Tsc2* were robustly co-labeled with S6 phosphorylation in the brain sections (Figure S11F and S11G). Together, these results suggest that in utero application of the CRISPR-Cas9 system is able to induce somatic loss-of-function mutations that affect the TSC complex in the focal cortical region similarly to those seen in individuals with FCDII.

Mosaic Knockout of *Tsc1* and *Tsc2* in the Focal Cortical Region Recapitulates the Clinical and Pathological Phenotypes Observed in Individuals with FCDII

Next, we investigated whether such a small fraction of neuronal cells exposed to selected sgRNAs with Cas9 could induce FCDII phenotypes such as migration defects, cytomegalic neurons, and spontaneous seizures in mice during the postnatal stage. After in utero electroporation of plasmids encoding Cas9 and sgRNA at E14, we selected P0 mouse pups that expressed red fluorescence signal in the focal cortical region and investigated FCDII-related phenotypes in these mice at >P21 (Figure 4A). First, we examined their cortical radial migration and found that dsRed-positive cells were significantly decreased in cortical layer II/III and increased in layers IV and V/VI, indicating that the radial migration of cortical neurons was abrogated (Figures 4B and 4C). Next, we began continuous video-EEG monitoring of the selected mice at 3 weeks. The selected mice were monitored by video-recording (12 hr/day) until convulsive spontaneous seizures were observed. If the mice had spontaneous behavioral seizures, we monitored them by video-EEG for 12 hr/day for >2 days to measure the frequency of the spontaneous seizures. Unexpectedly, the mice carrying the CRISPR construct targeting *Tsc1* or *Tsc2* displayed generalized tonic-clonic seizures, consistent with the symptoms of the individuals with FCDII (Figure 4D). Interestingly, even ~1% of the neuronal cells expressing the CRISPR-Cas9 construct were sufficient to induce spontaneous convulsive seizures (Figure 4B and Movie S1 and S2). The EEG pattern of the tonic and clonic phases displayed a low amplitude and fast spike, respectively, instead of a relatively high amplitude and spike-wave pattern, respectively (Figures 4D and S12). However, spontaneous seizures with ictal discharges were not observed in control mice electroporated with the control CRISPR-Cas9 plasmid without sgRNA expression (Figures 4E and S13). The frequency of spontaneous seizures was approximately ten events per day (Figure 4E). Approximately 50% of the selected mice expressing the *Tsc1*- or *Tsc2*-targeted CRISPR-Cas9 plasmid displayed spontaneous behavioral seizures with epileptic discharge (Figure S13). Furthermore, spontaneous seizures in *Tsc2* fKO mice were almost completely rescued by rapamycin treatment (Figure 4F). Finally, we examined whether the neuronal

(B) In utero electroporation of CRISPR vectors expressing selected sgRNA disrupts neuronal migration in the developing mouse neocortex. The images show coronal sections of mouse brains (>P56) electroporated with the CRISPR construct. We counted the percentage of dsRed (+) cells by dividing the number of dsRed (+) cells by the total number of cells (n = 2~3 per group). Scale bars, 250 μm.
(C) Bar charts showing the relative fluorescence intensities reflecting the distribution of electroporated cells within the cortex. Mice electroporated with the CRISPR construct without sgRNA expression served as controls. Data represent the mean ± SEM (n = 3–6 per group). *$p < 0.05$ and ***$p < 0.001$ compared with the control (two-way ANOVA with a Bonferroni multiple-comparison test).
(D) The EEG wave pattern in the ictal phase of *Tsc1* and *Tsc2* focal knockout (fKO) mice. EEG signals were recorded from four epidural electrodes located on the left frontal lobe (LF), right frontal lobe (RF), left temporal lobe (LT), and right temporal lobe (RT). Magnified EEG waves of the ictal phase and postictal period are presented in Figure S12.
(E) The seizure frequency in genome-edited mice was measured. Control mice were transfected with a CRISPR construct without sgRNA. Data represent the mean ± SEM (n = 3–6 per group).
(F) The seizure frequency in mice carrying the CRISPR construct targeting *Tsc2* was dramatically reduced by rapamycin treatment. Data represent the mean ± SEM (n = 4–12 per group). *$p < 0.05$ and **$p < 0.01$ compared with the control (one-way ANOVA with a Bonferroni post-test).

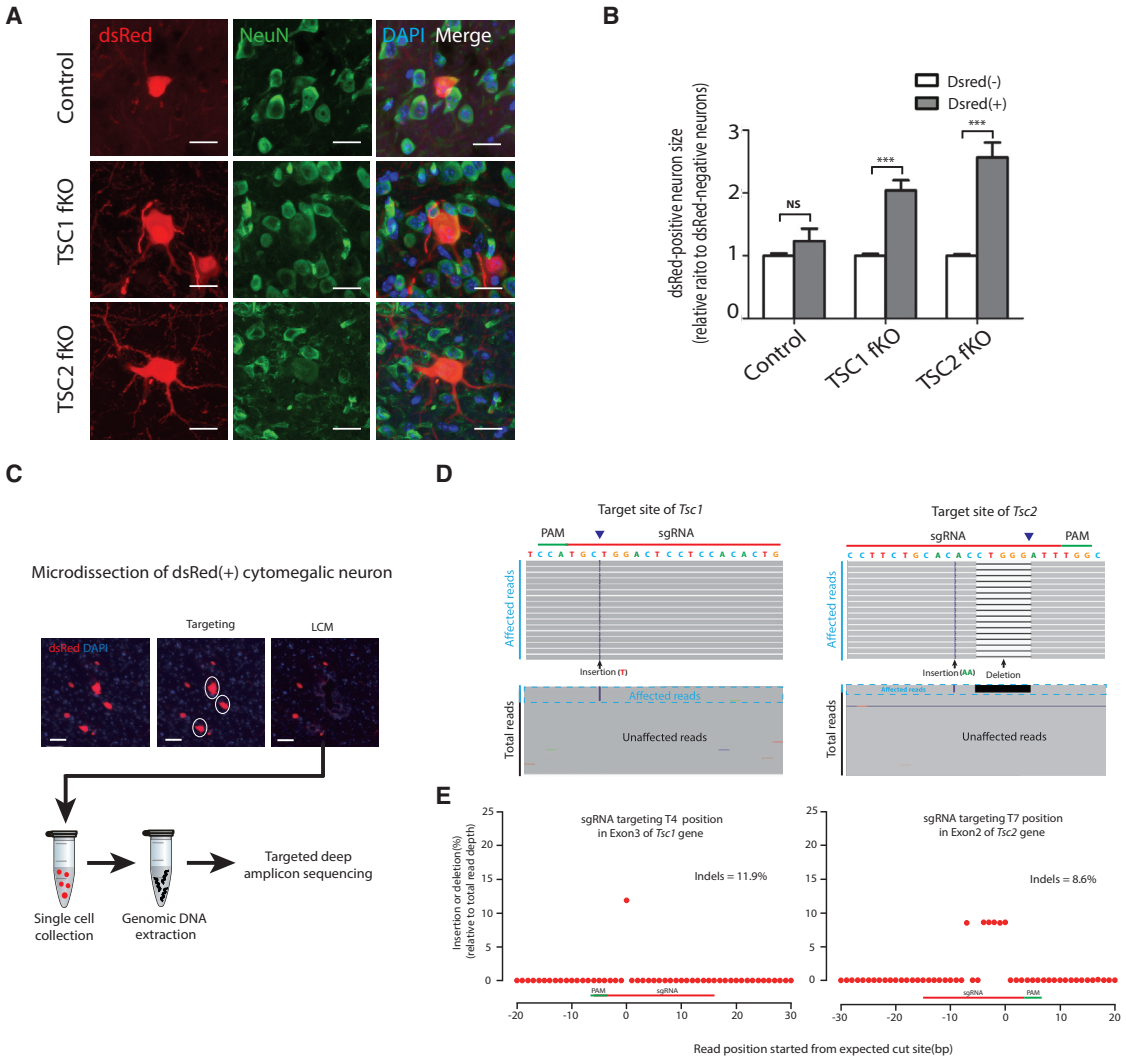

Figure 5. Cytomegalic Neurons Contain the Correctly Edited Genome Sequence of *Tsc1* and *Tsc2* Targeted by the CRISPR-Cas9 Construct

(A) Co-immunostaining for NeuN and DAPI. NeuN staining of dsRed-positive cells is presented. The soma size of dsRed-positive neurons was measured. Scale bars, 20 μm.

(B) Bar chart of the neuronal size in each group shows an increased soma size in affected cortical regions. Data represent the mean ± SEM (n = 27–299 per group). ***$p < 0.001$ compared with dsRed-negative neurons (Student's t test).

(C) Schematic figure of the microdissection procedure used to isolate dsRed-positive cytomegalic neurons and subsequent targeted deep amplicon sequencing. The dsRed-positive cytomegalic neurons are denoted by a white circle in the LCM image ("targeting"). Labeled neurons were microdissected, and 10~20 cells were collected in an adhesive cap tube. Genomic DNA was then extracted from the collected cells and submitted for deep amplicon sequencing. Scale bars, 50 μm.

(D) Representative view of *Tsc1* and *Tsc2* indels induced by *Tsc1* and *Tsc2* target sgRNA from the Integrative Genomic Viewer. Black and purple bars indicate deletions and insertions, respectively. The arrowheads indicate the theoretical cutting site of Cas9. PAM, protospacer adjacent motif.

(E) The frequency (relative to total reads) and position of indels are shown. The 0 position indicates the theoretical cutting site of Cas9 guided by sgRNA. The detailed amplicon sequencing procedure and deep sequencing data for the control group are presented in Figure S14.

cells electroporated with the CRISPR construct displayed dysmorphic neuronal phenotypes. Immunostaining of mouse brain sections revealed robust increases in the sizes of dsRed-positive neurons in affected cortical regions of the electroporated mice (Figures 5A and 5B). Furthermore, we tested whether the dsRed-positive neurons contained the correctly edited genome sequence targeted by the CRISPR-Cas9 construct. Using LCM, we microdissected the dsRed-positive dysmorphic neurons and subsequently performed site-specific deep sequencing (read depth of 49,224×~692,061×) around the sgRNA target site (Figures 5C and S14A). We observed that our in utero CRISPR-Cas9 system induced indels at the proper genomic position in *Tsc1* and *Tsc2*, corresponding to 3~4 nucleotides upstream of the PAM sequence of sgRNA and generating a frameshift mutation in the target genes, which resulted in functional

knockout. The percentage of mutated reads containing an insertion or deletion ranged from 8.6% to 11.9% (Figures 5D and 5E). However, no deletions or insertions were observed in mice that had been electroporated with the CRISPR construct without sgRNA expression (Figure S14B and S14C). Importantly, dysmorphic neurons in mice carrying the CRISPR construct targeting *Tsc2* were rescued by rapamycin treatment (Figure S15). Together, these data suggest that the mosaic knockout of *Tsc1* and *Tsc2* via in utero CRISPR-Cas9 application is sufficient to cause spontaneous behavioral seizures, as well as cytomegalic neurons and defective neuronal migration.

In Utero Application of Cas9n with Modified ssODN Models the Mutation of Individuals with FCD via HDR-Mediated Genome Editing

Although our focal *Tsc1* or *Tsc2* knockout mice recapitulated the FCDII phenotype, this in vivo genome-editing strategy did not result in the single-nucleotide substitution observed in individuals with FCDII. To model such a single-nucleotide substitution, it is necessary to edit a target base at the in vivo level via HDR-mediated genome editing. Current strategies for editing a target base by HDR remain very inefficient with a typically efficiency of ~0.1%–5%.[30,53] For in vivo modeling of a human somatic mutation, it is very unlikely that a single-nucleotide substitution with such an extremely low editing efficiency in the focal area of the mouse brain will induce behavioral changes such as epilepsy. In addition, it is necessary to avoid NHEJ-mediated *Tsc1* or *Tsc2* indels that induce hyperactivation of the mTOR pathway. Thus, we focused on characterizing changes in cell morphology, such as cytomegalic neurons and minimizing indels, after in utero somatic genome editing. To generate a mouse model carrying the mutation seen in individuals with FCDII—TSC2 p.Val1526Ile (GenBank: NM_011647.3) without indels—we performed in utero electroporation of Cas9n[30,54] combined with modified ssODNs with a modification,[36] which can increase the efficiency of HDR-mediated genome editing. First, to validate this method at the in vitro level, we co-transfected Neuro2A cells with Cas9n and sgRNA targeting TSC2 p.Val1526Ile, modified ssODNs as the donor, and performed RFLP analysis and high-throughput sequencing. We found that the group of nickase combined with modified ssODNs showed the best HDR efficiency (~5%) without indels (Figure S16). Next, we attempted in utero application of this method in the developing mouse brain. We electroporated mixed constructs (described above) with a dsRed reporter vector into the embryonic mouse brain at E14 and assessed at P28 whether this application caused changes in cellular morphology. Surprisingly, we were able to identify a small subset of dsRed-positive neurons that exhibited a cytomegalic morphology (Figures 6A and 6B). Next, we enriched these cytomegalic neurons by LCM, performed deep sequencing, and confirmed that these cytomegalic neurons carried the *Tsc2* c.4576G>A (p.Val1526Ile) mutation without indels (Figures 6B–6D). These results suggest that our in utero somatic genome editing by the CRISPR-Cas9 system faithfully recapitulated a single-nucleotide substitution and the important pathological feature observed in individuals with FCDII.

Discussion

Increasing evidence supports the pathogenic roles of somatic mutations in the brain in neurodevelopmental disorders such as FCD and HME, which lead to intractable epilepsy.[8,9,55,56] In previous studies, we and other groups have shown that brain somatic mutations in *MTOR* genes account for up to 25% of individuals with FCDII.[8,9,17] However, the genetic etiologies of the remaining FCDII individuals who lack *MTOR* mutations remain poorly understood. Here, we have provided evidence that brain somatic mutations in *TSC1* and *TSC2* account for 12.5% of the remaining FCDII individuals (5 of 40) who are negative for *MTOR* mutations. All of the identified mutations induced aberrant activation of mTOR kinase by disturbing the formation or function of the TSC1-TSC2 complex. Moreover, using the in utero CRISPR-Cas9 somatic genome-editing system, we clearly demonstrated that a focal cortical disruption of the TSC1-TSC2 complex, encoded by *Tsc1* and *Tsc2*, was sufficient to cause spontaneous behavioral seizures as well as migration defects and cytomegalic neurons, which are consistent with the neuropathological phenotype of individuals with FCDII. Moreover, in vivo modeling of the mutation identified in FCD individuals via HDR-mediated genome editing was able to recapitulate the abnormal neuronal morphology observed in FCD individuals.

Recent advances in deep sequencing technologies and bioinformatics analysis have provided evidence for brain somatic mutations or somatic mosaicism in neurodevelopmental disorders.[55–59] However, in vivo modeling of somatic mutations in the developing brain has been challenging given the limitations of genome-editing tools[60] and the size constraints of viral vectors.[61] In the present study, we combined in utero electroporation with the CRISPR-Cas9 system to introduce somatic genome modifications in a small fraction of neurons in the developing brain. In utero somatic genome editing of *Tsc1* and *Tsc2* faithfully recapitulated not only the abnormal neuronal phenotypes but also the neurobehavioral deficits observed in individuals with FCDII. Although there have been a few examples of the use of in utero electroporation of CRISPR-Cas9 in mice for modeling brain tumors,[62] studying NMDA receptor functions in the synapses of hippocampal neurons,[63] and disrupting neurogenesis in the embryonic brain without causing any neurobehavioral deficits in mice,[64] our mouse model of CRISPR-Cas9-mediated brain somatic mutations causing a neurodevelopmental disorder has successfully recapitulated neurobehavioral deficits such as spontaneous epileptic seizures in FCD-affected individuals. Recently, combining the in utero

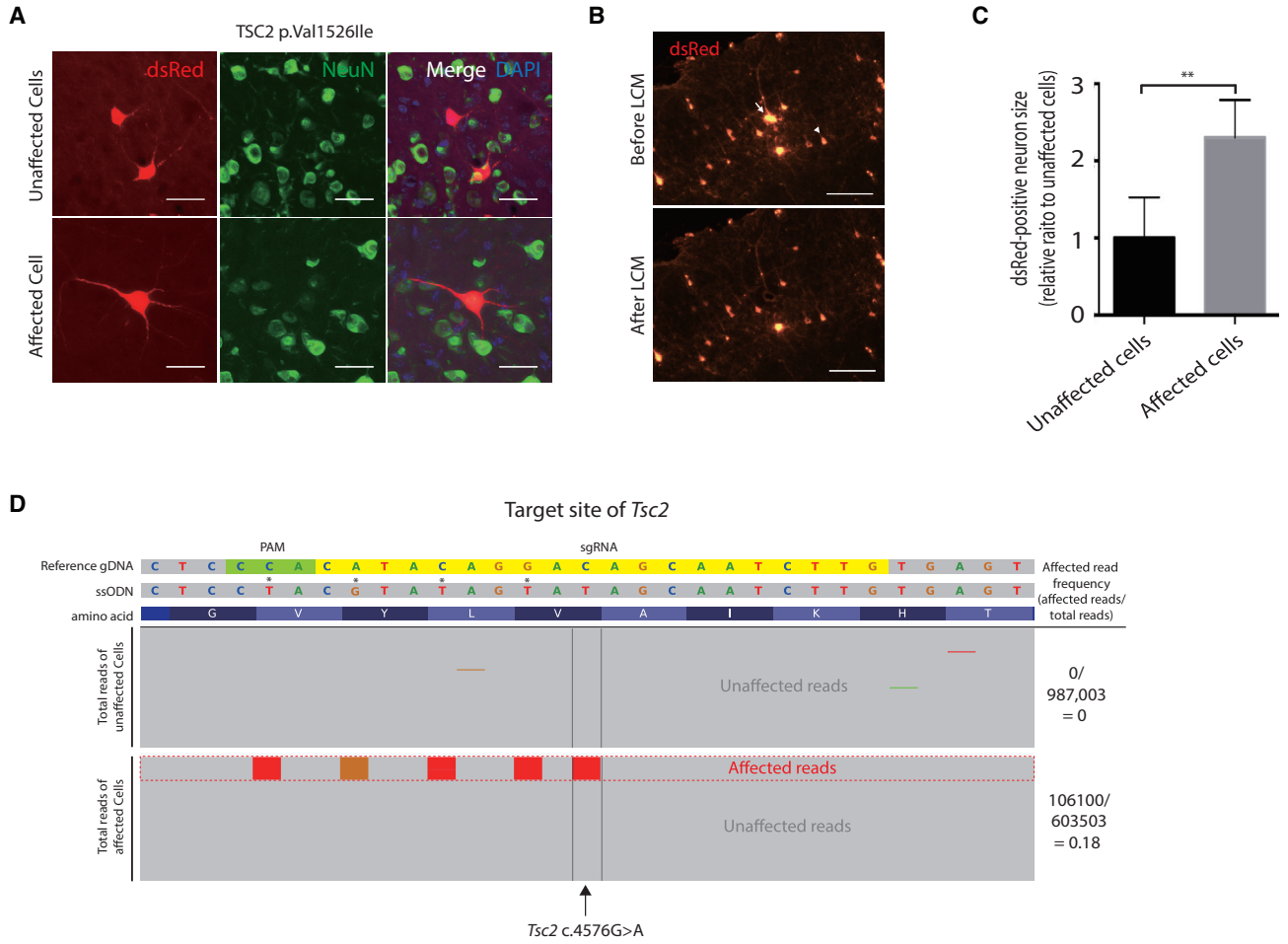

Figure 6. In Utero Application of Cas9n with Modified ssODN Models Cytomegalic Neurons Carrying the TSC2 p.Val1526Ile Variant
(A) Co-immunostaining for NeuN and DAPI in mouse brains at P28, which were electroporated in utero with Cas9n-selected sgRNA and modified single-stranded oligonucleotides (ssODNs) targeting mouse TSC2 c.4576G>A (p.Val1526Ile), corresponding to human TSC2 c.4639G>A (p.Val1547Ile). Among the dsRed-positive neurons, a small subset of cytomegalic neurons ("affected cells") were observed. Scale bars, 25 μm.
(B) LCM was used to isolate dsRed-positive cytomegalic neurons. We discerned the affected cells from the unaffected cells by carefully examining the cell size. Prior to capturing the cells, we analyzed the image and selected target cells with a size two times larger than the average neuron size. The white arrowhead and arrow indicate the unaffected and affected cells, respectively. Scale bars, 100 μm.
(C) Bar chart of the neuronal size in unaffected and affected cells. Data represent the mean ± SEM (n = 10–21 per group). **$p < 0.01$ compared with dsRed-positive unaffected neurons (Student's t test).
(D) Representative view of *Tsc2* targeted by modified ssODNs from the collapsed view of the Integrative Genomic Viewer. The green and yellow bars on the reference genomic sequence indicate the PAM and the target site of sgRNA, respectively. To discerned HDR from random mutations, we inserted several point mutations in ssODNs (asterisk) to induce silence mutations.

electroporation technique with the Cre-LoxP system was able to recapitulate several key features of the focal cortical malformation (FCM) in humans, including dyslamination and the presence of cytomegalic neurons.[22] However, in this model, it usually takes a long time to establish mouse lines with the Cre-LoxP system. Importantly, this model was not able to recapitulate the spontaneous seizure activity. In the present work, the mouse model generated with the in utero CRISPR system showed spontaneous seizure activity, which is a key feature of FCM, and thus more closely recapitulated the symptoms of individuals with FCD.

Recently, the ExAC Browser has been introduced as an useful reference for examining the allele frequency of mutations in large populations.[65] Because relatively common variants are unlikely to cause disease, the allele frequency of identified mutations in the ExAC Browser is important for determining pathogenicity. However, the ExAC Browser is known to include individuals with disease and contain rare pathogenic variants (MAF $< 1 \times 10^{-4}$).[66] Indeed, the *TSC2* c.292C>T mutation identified from the blood of TSC individuals is listed in the ExAC Browser (rs372321790; MAF $= 2.99 \times 10^{-5}$). This mutation was previously reported to disrupt TSC2 function and was classified as pathogenic.[67] In addition, loss-of-function variants, such as TSC1 p.Gln4* (MAF $= 8.25 \times 10^{-6}$), TSC2 p.Gln1284* (MAF $= 3.34 \times 10^{-5}$), and TSC2 p.Cys21* (MAF $= 6.62 \times 10^{-5}$), are also listed in the ExAC Browser. Therefore, the allele frequency of identified mutations in

the ExAC Browser should be considered a supportive evaluation method for determining the pathogenicity.

Current bioinformatic analysis tools for detecting low-level somatic mutations have a technical limitation in detecting low-level indels, which can frequently cause frameshift or truncating mutations. Therefore, the current analysis of low-level somatic mutations is biased to detect single-nucleotide changes that can cause pathogenic missense mutations or nonsense (stop-gain) mutations. If advanced genome analysis tools for detecting low-level indels are available in the future, additional low-frequency somatic *TSC1* and *TSC2* mutations (frameshift) could be found in FCDII samples.

It has recently been reported that familial cortical dysplasia is associated with germline mutations in *DEPDC5* (MIM: 614191) and *NPRL3* (MIM: 600928), which suppress mTOR signaling.[68,69] One FCDII individual demonstrated a somatic mutation in *PIK3CA*.[70] HME, which shares neuropathological features such as cytomegalic neurons and cortical dyslamination with FCDII, are also known to be associated with somatic mutations in *PIK3CA*, *PIK3R2*, *AKT3*, and *MTOR*, as well as germline mutations in *PTEN* and *TSC2*.[17,70] These genes encode well-known regulators of the mTOR pathway, and their dysfunction can lead to aberrant activation of mTOR kinase. Together, these findings and the present results strongly suggest that hyperactivation of mTOR kinase by mutations in mTOR pathway genes underlies the molecular pathogenesis of FCD, which is the most common form of childhood intractable epilepsy and requires surgery as a treatment. These findings also suggest that hyperactivated mTOR kinase is a therapeutic and genetically validated target in individuals with FCD.[8] Although the genetic etiology and molecular pathogenesis of FCD remain to be fully defined, our study has not only revealed additional somatic mosaic mutations that lead to FCD but also described the generation of a mouse model with brain somatic mutations via in utero somatic genome-editing technology. This study will provide a foundation for future clinical and scientific research of FCD.

Accession Numbers

The sequencing data of individuals with variants reported in this paper have been deposited in the Sequence Read Archive under accession number SRA: PRJNA369620.

Supplemental Data

Supplemental Data include 16 figures, 10 tables, and 2 movies and can be found with this article online at http://dx.doi.org/10.1016/j.ajhg.2017.01.030.

Acknowledgments

We thank Dr. Sun Min Park at the Korea Advanced Institute of Science and Technology (KAIST) for coordinating clinical information. This work was supported by the Korean Health Technology R&D Project of the Korean Ministry of Health & Welfare (grants H15C3143 and H16C0415 to J.H.L., HI14C1588 and HI15C1601 to H.C.K., and HI14C2019 to H.K.); Citizens United for Research in Epilepsy (J.H.L.); the Brain Research Program through the National Research Foundation of Korea, funded by the Ministry of Science, ICT, and Future Planning (grants 2013M3C7A1056564 to J.H.L. and 2015R1A2A1A15052668 to H.K.); and the KAIST Future Systems Healthcare Project from the Ministry of Science, ICT, and Future Planning (J.H.L.).

Received: September 22, 2016
Accepted: January 23, 2017
Published: February 16, 2017

Web Resources

1000 Genomes, http://browser.1000genomes.org
Burrows-Wheeler Aligner, http://bio-bwa.sourceforge.net
EEGLAB, http://sccn.ucsd.edu/eeglab
Exome Aggregate Consortium (ExAC) Browser, http://exac.broadinstitute.org
GATK, http://www.broadinstitute.org/gatk
Illumina DesignStudio, http://www.illumina.com/designstudio
ImageJ, http://rsbweb.nih.gov/ij
LOVD Tuberous Sclerosis Database, http://chromium.lovd.nl/LOVD2/TSC
OMIM, http://www.omim.org
RefSeq, http://www.ncbi.nlm.nih.gov/refseq/
SAMtools, http://samtools.sourceforge.net
Sequence Read Archive (SRA), https://www.ncbi.nlm.nih.gov/sra

References

1. Blümcke, I., Vinters, H.V., Armstrong, D., Aronica, E., Thom, M., and Spreafico, R. (2009). Malformations of cortical development and epilepsies: neuropathological findings with emphasis on focal cortical dysplasia. Epileptic Disord. *11*, 181–193.
2. Sisodiya, S.M. (2000). Surgery for malformations of cortical development causing epilepsy. Brain *123*, 1075–1091.
3. Bast, T., Ramantani, G., Seitz, A., and Rating, D. (2006). Focal cortical dysplasia: prevalence, clinical presentation and epilepsy in children and adults. Acta Neurol. Scand. *113*, 72–81.
4. Tassi, L., Colombo, N., Garbelli, R., Francione, S., Lo Russo, G., Mai, R., Cardinale, F., Cossu, M., Ferrario, A., Galli, C., et al. (2002). Focal cortical dysplasia: neuropathological subtypes, EEG, neuroimaging and surgical outcome. Brain *125*, 1719–1732.
5. Fauser, S., Huppertz, H.J., Bast, T., Strobl, K., Pantazis, G., Altenmueller, D.M., Feil, B., Rona, S., Kurth, C., Rating, D., et al. (2006). Clinical characteristics in focal cortical dysplasia: a retrospective evaluation in a series of 120 patients. Brain *129*, 1907–1916.
6. Fauser, S., Schulze-Bonhage, A., Honegger, J., Carmona, H., Huppertz, H.J., Pantazis, G., Rona, S., Bast, T., Strobl, K., Steinhoff, B.J., et al. (2004). Focal cortical dysplasias: surgical outcome in 67 patients in relation to histological subtypes and dual pathology. Brain *127*, 2406–2418.
7. Zech, R., Kiontke, S., Mueller, U., Oeckinghaus, A., and Kümmel, D. (2016). Structure of the Tuberous Sclerosis Complex 2 (TSC2) N Terminus Provides Insight into Complex Assembly and Tuberous Sclerosis Pathogenesis. J. Biol. Chem. *291*, 20008–20020.

8. Lim, J.S., Kim, W.-I., Kang, H.C., Kim, S.H., Park, A.H., Park, E.K., Cho, Y.-W., Kim, S., Kim, H.M., Kim, J.A., et al. (2015). Brain somatic mutations in MTOR cause focal cortical dysplasia type II leading to intractable epilepsy. Nat. Med. *21*, 395–400.
9. Nakashima, M., Saitsu, H., Takei, N., Tohyama, J., Kato, M., Kitaura, H., Shiina, M., Shirozu, H., Masuda, H., Watanabe, K., et al. (2015). Somatic Mutations in the MTOR gene cause focal cortical dysplasia type IIb. Ann. Neurol. *78*, 375–386.
10. Costa-Mattioli, M., and Monteggia, L.M. (2013). mTOR complexes in neurodevelopmental and neuropsychiatric disorders. Nat. Neurosci. *16*, 1537–1543.
11. Wong, M., and Crino, P.B. (2012). In SourceJasper's Basic Mechanisms of the Epilepsies, Fourth Edition, J.L. Noebels, M. Avoli, M.A. Rogawski, R.W. Olsen, and A.V. Delgado-Escueta, eds. (National Center for Biotechnology Information).
12. Laplante, M., and Sabatini, D.M. (2012). mTOR signaling in growth control and disease. Cell *149*, 274–293.
13. Aronica, E., Boer, K., Baybis, M., Yu, J., and Crino, P. (2007). Co-expression of cyclin D1 and phosphorylated ribosomal S6 proteins in hemimegalencephaly. Acta Neuropathol. *114*, 287–293.
14. Baybis, M., Yu, J., Lee, A., Golden, J.A., Weiner, H., McKhann, G., 2nd, Aronica, E., and Crino, P.B. (2004). mTOR cascade activation distinguishes tubers from focal cortical dysplasia. Ann. Neurol. *56*, 478–487.
15. Ljungberg, M.C., Bhattacharjee, M.B., Lu, Y., Armstrong, D.L., Yoshor, D., Swann, J.W., Sheldon, M., and D'Arcangelo, G. (2006). Activation of mammalian target of rapamycin in cytomegalic neurons of human cortical dysplasia. Ann. Neurol. *60*, 420–429.
16. Miyata, H., Chiang, A.C.Y., and Vinters, H.V. (2004). Insulin signaling pathways in cortical dysplasia and TSC-tubers: tissue microarray analysis. Ann. Neurol. *56*, 510–519.
17. D'Gama, A.M., Geng, Y., Couto, J.A., Martin, B., Boyle, E.A., LaCoursiere, C.M., Hossain, A., Hatem, N.E., Barry, B.J., Kwiatkowski, D.J., et al. (2015). Mammalian target of rapamycin pathway mutations cause hemimegalencephaly and focal cortical dysplasia. Ann. Neurol. *77*, 720–725.
18. Inoki, K., Corradetti, M.N., and Guan, K.L. (2005). Dysregulation of the TSC-mTOR pathway in human disease. Nat. Genet. *37*, 19–24.
19. Lee, J.H., Huynh, M., Silhavy, J.L., Kim, S., Dixon-Salazar, T., Heiberg, A., Scott, E., Bafna, V., Hill, K.J., Collazo, A., et al. (2012). De novo somatic mutations in components of the PI3K-AKT3-mTOR pathway cause hemimegalencephaly. Nat. Genet. *44*, 941–945.
20. Qin, W., Kozlowski, P., Taillon, B.E., Bouffard, P., Holmes, A.J., Janne, P., Camposano, S., Thiele, E., Franz, D., and Kwiatkowski, D.J. (2010). Ultra deep sequencing detects a low rate of mosaic mutations in tuberous sclerosis complex. Hum. Genet. *127*, 573–582.
21. Tyburczy, M.E., Dies, K.A., Glass, J., Camposano, S., Chekaluk, Y., Thorner, A.R., Lin, L., Krueger, D., Franz, D.N., Thiele, E.A., et al. (2015). Mosaic and Intronic Mutations in TSC1/TSC2 Explain the Majority of TSC Patients with No Mutation Identified by Conventional Testing. PLoS Genet. *11*, e1005637.
22. Feliciano, D.M., Su, T., Lopez, J., Platel, J.-C., and Bordey, A. (2011). Single-cell Tsc1 knockout during corticogenesis generates tuber-like lesions and reduces seizure threshold in mice. J. Clin. Invest. *121*, 1596–1607.
23. Doudna, J.A., and Charpentier, E. (2014). Genome editing. The new frontier of genome engineering with CRISPR-Cas9. Science *346*, 1258096.
24. Kim, H., and Kim, J.S. (2014). A guide to genome engineering with programmable nucleases. Nat. Rev. Genet. *15*, 321–334.
25. Blümcke, I., Thom, M., Aronica, E., Armstrong, D.D., Vinters, H.V., Palmini, A., Jacques, T.S., Avanzini, G., Barkovich, A.J., Battaglia, G., et al. (2011). The clinicopathologic spectrum of focal cortical dysplasias: a consensus classification proposed by an ad hoc Task Force of the ILAE Diagnostic Methods Commission. Epilepsia *52*, 158–174.
26. Kim, Y.H., Kang, H.C., Kim, D.S., Kim, S.H., Shim, K.W., Kim, H.D., and Lee, J.S. (2011). Neuroimaging in identifying focal cortical dysplasia and prognostic factors in pediatric and adolescent epilepsy surgery. Epilepsia *52*, 722–727.
27. Northrup, H., Krueger, D.A.; and International Tuberous Sclerosis Complex Consensus Group (2013). Tuberous sclerosis complex diagnostic criteria update: recommendations of the 2012 Iinternational Tuberous Sclerosis Complex Consensus Conference. Pediatr. Neurol. *49*, 243–254.
28. Shirley, M.D., Tang, H., Gallione, C.J., Baugher, J.D., Frelin, L.P., Cohen, B., North, P.E., Marchuk, D.A., Comi, A.M., and Pevsner, J. (2013). Sturge-Weber syndrome and port-wine stains caused by somatic mutation in GNAQ. N. Engl. J. Med. *368*, 1971–1979.
29. Kuilman, T., Velds, A., Kemper, K., Ranzani, M., Bombardelli, L., Hoogstraat, M., Nevedomskaya, E., Xu, G., de Ruiter, J., Lolkema, M.P., et al. (2015). CopywriteR: DNA copy number detection from off-target sequence data. Genome Biol. *16*, 49.
30. Cong, L., Ran, F.A., Cox, D., Lin, S., Barretto, R., Habib, N., Hsu, P.D., Wu, X., Jiang, W., Marraffini, L.A., and Zhang, F. (2013). Multiplex genome engineering using CRISPR/Cas systems. Science *339*, 819–823.
31. Ramakrishna, S., Kwaku Dad, A.B., Beloor, J., Gopalappa, R., Lee, S.K., and Kim, H. (2014). Gene disruption by cell-penetrating peptide-mediated delivery of Cas9 protein and guide RNA. Genome Res. *24*, 1020–1027.
32. Kim, H.J., Lee, H.J., Kim, H., Cho, S.W., and Kim, J.S. (2009). Targeted genome editing in human cells with zinc finger nucleases constructed via modular assembly. Genome Res. *19*, 1279–1288.
33. Kim, Y.H., Ramakrishna, S., Kim, H., and Kim, J.S. (2014). Enrichment of cells with TALEN-induced mutations using surrogate reporters. Methods *69*, 108–117.
34. Guschin, D.Y., Waite, A.J., Katibah, G.E., Miller, J.C., Holmes, M.C., and Rebar, E.J. (2010). A rapid and general assay for monitoring endogenous gene modification. Methods Mol. Biol. *649*, 247–256.
35. Ramakrishna, S., Cho, S.W., Kim, S., Song, M., Gopalappa, R., Kim, J.S., and Kim, H. (2014). Surrogate reporter-based enrichment of cells containing RNA-guided Cas9 nuclease-induced mutations. Nat. Commun. *5*, 3378.
36. Renaud, J.B., Boix, C., Charpentier, M., De Cian, A., Cochennec, J., Duvernois-Berthet, E., Perrouault, L., Tesson, L., Edouard, J., Thinard, R., et al. (2016). Improved Genome Editing Efficiency and Flexibility Using Modified Oligonucleotides with TALEN and CRISPR-Cas9 Nucleases. Cell Rep. *14*, 2263–2272.
37. Au, K.S., Williams, A.T., Roach, E.S., Batchelor, L., Sparagana, S.P., Delgado, M.R., Wheless, J.W., Baumgartner, J.E., Roa, B.B., Wilson, C.M., et al. (2007). Genotype/phenotype

correlation in 325 individuals referred for a diagnosis of tuberous sclerosis complex in the United States. Genet. Med. *9*, 88–100.
38. Saunders, C.T., Wong, W.S.W., Swamy, S., Becq, J., Murray, L.J., and Cheetham, R.K. (2012). Strelka: accurate somatic small-variant calling from sequenced tumor-normal sample pairs. Bioinformatics *28*, 1811–1817.
39. Ratan, A., Miller, W., Guillory, J., Stinson, J., Seshagiri, S., and Schuster, S.C. (2013). Comparison of sequencing platforms for single nucleotide variant calls in a human sample. PLoS ONE *8*, e55089.
40. Lam, H.Y.K., Clark, M.J., Chen, R., Chen, R., Natsoulis, G., O'Huallachain, M., Dewey, F.E., Habegger, L., Ashley, E.A., Gerstein, M.B., et al. (2011). Performance comparison of whole-genome sequencing platforms. Nat. Biotechnol. *30*, 78–82.
41. Lin, D.C., Meng, X., Hazawa, M., Nagata, Y., Varela, A.M., Xu, L., Sato, Y., Liu, L.Z., Ding, L.W., Sharma, A., et al. (2014). The genomic landscape of nasopharyngeal carcinoma. Nat. Genet. *46*, 866–871.
42. Huang, J., and Manning, B.D. (2008). The TSC1-TSC2 complex: a molecular switchboard controlling cell growth. Biochem. J. *412*, 179–190.
43. Benvenuto, G., Li, S., Brown, S.J., Braverman, R., Vass, W.C., Cheadle, J.P., Halley, D.J., Sampson, J.R., Wienecke, R., and DeClue, J.E. (2000). The tuberous sclerosis-1 (TSC1) gene product hamartin suppresses cell growth and augments the expression of the TSC2 product tuberin by inhibiting its ubiquitination. Oncogene *19*, 6306–6316.
44. Chong-Kopera, H., Inoki, K., Li, Y., Zhu, T., Garcia-Gonzalo, F.R., Rosa, J.L., and Guan, K.L. (2006). TSC1 stabilizes TSC2 by inhibiting the interaction between TSC2 and the HERC1 ubiquitin ligase. J. Biol. Chem. *281*, 8313–8316.
45. Li, Y., Inoki, K., and Guan, K.L. (2004). Biochemical and functional characterizations of small GTPase Rheb and TSC2 GAP activity. Mol. Cell. Biol. *24*, 7965–7975.
46. Lozovaya, N., Gataullina, S., Tsintsadze, T., Tsintsadze, V., Pallesi-Pocachard, E., Minlebaev, M., Goriounova, N.A., Buhler, E., Watrin, F., Shityakov, S., et al. (2014). Selective suppression of excessive GluN2C expression rescues early epilepsy in a tuberous sclerosis murine model. Nat. Commun. *5*, 4563.
47. Sancak, O., Nellist, M., Goedbloed, M., Elfferich, P., Wouters, C., Maat-Kievit, A., Zonnenberg, B., Verhoef, S., Halley, D., and van den Ouweland, A. (2005). Mutational analysis of the TSC1 and TSC2 genes in a diagnostic setting: genotype–phenotype correlations and comparison of diagnostic DNA techniques in Tuberous Sclerosis Complex. Eur. J. Hum. Genet. *13*, 731–741.
48. Wong, M. (2015). Tuber-Less Models of Tuberous Sclerosis Still Provide Insights Into Epilepsy. Epilepsy Curr. *15*, 129–130.
49. Hoogeveen-Westerveld, M., Ekong, R., Povey, S., Karbassi, I., Batish, S.D., den Dunnen, J.T., van Eeghen, A., Thiele, E., Mayer, K., Dies, K., et al. (2012). Functional assessment of TSC1 missense variants identified in individuals with tuberous sclerosis complex. Hum. Mutat. *33*, 476–479.
50. Mozaffari, M., Hoogeveen-Westerveld, M., Kwiatkowski, D., Sampson, J., Ekong, R., Povey, S., den Dunnen, J.T., van den Ouweland, A., Halley, D., and Nellist, M. (2009). Identification of a region required for TSC1 stability by functional analysis of TSC1 missense mutations found in individuals with tuberous sclerosis complex. BMC Med. Genet. *10*, 88.
51. Magri, L., Cominelli, M., Cambiaghi, M., Cursi, M., Leocani, L., Minicucci, F., Poliani, P.L., and Galli, R. (2013). Timing of mTOR activation affects tuberous sclerosis complex neuropathology in mouse models. Dis. Model. Mech. *6*, 1185–1197.
52. Zhang, H., Cicchetti, G., Onda, H., Koon, H.B., Asrican, K., Bajraszewski, N., Vazquez, F., Carpenter, C.L., and Kwiatkowski, D.J. (2003). Loss of Tsc1/Tsc2 activates mTOR and disrupts PI3K-Akt signaling through downregulation of PDGFR. J. Clin. Invest. *112*, 1223–1233.
53. Mikuni, T., Nishiyama, J., Sun, Y., Kamasawa, N., and Yasuda, R. (2016). High-Throughput, High-Resolution Mapping of Protein Localization in Mammalian Brain by In Vivo Genome Editing. Cell *165*, 1803–1817.
54. Ran, F.A., Hsu, P.D., Wright, J., Agarwala, V., Scott, D.A., and Zhang, F. (2013). Genome engineering using the CRISPR-Cas9 system. Nat. Protoc. *8*, 2281–2308.
55. Jamuar, S.S., Lam, A.-T.N., Kircher, M., D'Gama, A.M., Wang, J., Barry, B.J., Zhang, X., Hill, R.S., Partlow, J.N., Rozzo, A., et al. (2014). Somatic mutations in cerebral cortical malformations. N. Engl. J. Med. *371*, 733–743.
56. Poduri, A., Evrony, G.D., Cai, X., and Walsh, C.A. (2013). Somatic mutation, genomic variation, and neurological disease. Science *341*, 1237758.
57. Hu, W.F., Chahrour, M.H., and Walsh, C.A. (2014). The diverse genetic landscape of neurodevelopmental disorders. Annu. Rev. Genomics Hum. Genet. *15*, 195–213.
58. Kim, S., Jeong, K., Bhutani, K., Lee, J., Patel, A., Scott, E., Nam, H., Lee, H., Gleeson, J.G., and Bafna, V. (2013). Virmid: accurate detection of somatic mutations with sample impurity inference. Genome Biol. *14*, R90.
59. Lee, J.H. (2016). Somatic mutations in disorders with disrupted brain connectivity. Exp. Mol. Med. *48*, e239.
60. Gaj, T., Gersbach, C.A., and Barbas, C.F., 3rd. (2013). ZFN, TALEN, and CRISPR/Cas-based methods for genome engineering. Trends Biotechnol. *31*, 397–405.
61. Hsu, P.D., Lander, E.S., and Zhang, F. (2014). Development and applications of CRISPR-Cas9 for genome engineering. Cell *157*, 1262–1278.
62. Zuckermann, M., Hovestadt, V., Knobbe-Thomsen, C.B., Zapatka, M., Northcott, P.A., Schramm, K., Belic, J., Jones, D.T.W., Tschida, B., Moriarity, B., et al. (2015). Somatic CRISPR/Cas9-mediated tumour suppressor disruption enables versatile brain tumour modelling. Nat. Commun. *6*, 7391.
63. Straub, C., Granger, A.J., Saulnier, J.L., and Sabatini, B.L. (2014). CRISPR/Cas9-mediated gene knock-down in post-mitotic neurons. PLoS ONE *9*, e105584.
64. Kalebic, N., Taverna, E., Tavano, S., Wong, F.K., Suchold, D., Winkler, S., Huttner, W.B., and Sarov, M. (2016). CRISPR/Cas9-induced disruption of gene expression in mouse embryonic brain and single neural stem cells in vivo. EMBO Rep. *17*, 338–348.
65. Lek, M., Karczewski, K.J., Minikel, E.V., Samocha, K.E., Banks, E., Fennell, T., O'Donnell-Luria, A.H., Ware, J.S., Hill, A.J., Cummings, B.B., et al.; Exome Aggregation Consortium (2016). Analysis of protein-coding genetic variation in 60,706 humans. Nature *536*, 285–291.
66. Walsh, R., Thomson, K.L., Ware, J.S., Funke, B.H., Woodley, J., McGuire, K.J., Mazzarotto, F., Blair, E., Seller, A., Taylor, J.C., et al.; Exome Aggregation Consortium (2016). Reassessment of Mendelian gene pathogenicity using 7,855 cardiomyopathy cases and 60,706 reference samples. Genet. Med. Published online August 17, 2016.

67. Hoogeveen-Westerveld, M., Wentink, M., van den Heuvel, D., Mozaffari, M., Ekong, R., Povey, S., den Dunnen, J.T., Metcalfe, K., Vallee, S., Krueger, S., et al. (2011). Functional assessment of variants in the TSC1 and TSC2 genes identified in individuals with Tuberous Sclerosis Complex. Hum. Mutat. *32*, 424–435.
68. Baulac, S., Ishida, S., Marsan, E., Miquel, C., Biraben, A., Nguyen, D.K., Nordli, D., Cossette, P., Nguyen, S., Lambrecq, V., et al. (2015). Familial focal epilepsy with focal cortical dysplasia due to DEPDC5 mutations. Ann. Neurol. *77*, 675–683.
69. Sim, J.C., Scerri, T., Fanjul-Fernández, M., Riseley, J.R., Gillies, G., Pope, K., van Roozendaal, H., Heng, J.I., Mandelstam, S.A., McGillivray, G., et al. (2016). Familial cortical dysplasia caused by mutation in the mammalian target of rapamycin regulator NPRL3. Ann. Neurol. *79*, 132–137.
70. Jansen, L.A., Mirzaa, G.M., Ishak, G.E., O'Roak, B.J., Hiatt, J.B., Roden, W.H., Gunter, S.A., Christian, S.L., Collins, S., Adams, C., et al. (2015). PI3K/AKT pathway mutations cause a spectrum of brain malformations from megalencephaly to focal cortical dysplasia. Brain *138*, 1613–1628.